Lipid bilayers: phase behavior and nanomechanics

LORENA REDONDO-MORATA

Center for Infection and Immunity of Lille, INSERM U1019, CNRS UMR 8204, F-59000 Lille, France.

PATRICIA LOSADA-PÉREZ

Experimental Soft Matter and Thermal Physics (EST) group, Department of Physics, Université Libre de Bruxelles, 1050 Brussels, Belgium

MARINA INÉS GIANNOTTI

Biomedical Research Networking Center on Bioengineering, Biomaterials and Nanomedicine (CIBER-BBN), Spain.

Institut de Bioenginyeria de Catalunya (IBEC), The Barcelona Institute of Science and Technology (BIST), 08028 Barcelona, Spain.

Departament de Ciència de Materials i Química Física, Universitat de Barcelona, 08028 Barcelona, Spain.

migiannotti@ibecbarcelona.eu

Keywords:

Lipid phase behavior / phase transition / phase coexistence / nanomechanics / thermodynamics / Atomic Force Microscopy (AFM)/ Quartz crystal microbalance with dissipation monitoring (QCM-D)

Contents

1. Abstract

Lipid membranes are involved in many physiological processes like recognition, signaling, fusion or remodeling of the cell membrane or some of its internal compartments. Within the cell, they are the ultimate barrier, while maintaining the fluidity or flexibility required for a myriad of processes, including membrane protein assembly. The physical properties of *in vitro* model membranes as model cell membranes have been extensively studied with a variety of techniques, from classical thermodynamics to advanced modern microscopies. Here we review the nanomechanics of solid-supported lipid membranes with a focus in their phase behavior. Relevant information obtained by quartz crystal microbalance with dissipation monitoring (QCM-D) and atomic force microscopy (AFM) as complementary techniques in the nano/mesoscale interface is presented. Membrane morphological and mechanical characterization will be discussed in the framework of its phase behavior, phase transitions and coexistence, in simple and complex models, and upon the presence of cholesterol.

2. Introduction

Cells can be thermodynamically defined as open systems in constant exchange of mass, energy and information with the environment. The membrane is the ultimate boundary for the cell, confining it from the medium and some of its internal compartments. The cell membrane is a fundamental structure of the cell, providing a support matrix for proteins and carbohydrates. As complex systems, cell membrane performance is the result of lipids and proteins working together, with main functions like being barriers, mediating the exchange of molecules and information, promoting signaling and adhesion, and being metabolically self-renewing structures.

Cell membranes are materials with unique physical properties allowing cells to rapidly change shape, squeeze, stretch, pinch off smaller units, fuse, and reseal. This is the result of being viscous sheets with both fluid and elastic properties. Cell membranes are supramolecular structures, where the lipids and proteins interact through non-covalent bonding. Membranes are curved surfaces, vesicular in nature, whose curvature is deeply influenced by the lipid packing. The lipid bilayer, made of millions of building blocks held together by weak interactions, is in part responsible for the physical, dynamic and mechanical properties of the cell membrane. In the membrane, lipids are mainly organized in lamellar phases, where two leaflets of lipids are self-assembled exposing the polar headgroups to the aqueous interface and keeping the fatty-acyl chains aligned opposed and parallel to one another to form the hydrophobic core.

The enterprising scientist Alec Bangham was the discoverer in 1958 of the 'multilamellar smectic mesophases' or, as himself referred to less seriously, the 'bangasomes' (Bangham et al., 1958) - which were eventually named 'liposomes' to define microscopic lipid vesicles (Sessa & Weissmann, 1968). When the Babraham Institute (Cambridge, UK) acquired its first electron microscope in 1961, Bangham had the privilege to firstly observe the dispersions of phospholipids in water solutions of negative stains (Bangham & Horne, 1964). In the following years, Bangham and his collaborators performed the key experiments to demonstrate that lipid bilayers maintain concentration gradients of ions such as potassium and sodium. Indeed, David D. Deamer wrote in his memoir "*It was the membrane equivalent of finding the double helix structure of DNA, another Cambridge discovery in the life sciences*"(Deamer, 2010). This was reflected in the well-known lecture by Bangham in the University of Bristol in 1975, entitled "Membranes came first", where he proposed that something similar to liposomes had been available to house the first forms of life. Indeed, all living organisms have a membrane.

Later in the early 1970s, Singer and Nicolson proposed the fluid-mosaic-model, depicturing the cell membranes as two-dimensional liquids where all lipid and protein molecules diffuse easily (Singer & Nicolson, 1972). Concerning the composition, besides all the proteins and carbohydrates, lipids are the main components of the cell membrane in terms of molar fraction. Lipids are a broad family which covers many different chemical structure sphingolipids (ceramides, sphingomyelin, gangliosides, sphingosines), sterols (cholesterol and vitamins), and phospholipids, each of them contributing to different and crucial physicochemical properties.

Gradual progress was made in the knowledge of the complexity of the biological membranes. The most famous hypothesis in the field is the membrane raft proposed in 1997 by K. Simons and E. Ikonen (Simons & Ikonen, 1997). The idea was based on the fact that portions of membrane were found to be detergent resistant, that may give rise to a virtual compartmentalization of the cell. This hypothesis generated a lot of literature and became a recursive concept in the field. Nowadays it is well known that there is a variety of nanostructures in the membrane of heterogeneous sizes and functions, and the methods that allow us to observe these nanodomains *in vivo* are only beginning to emerge (Goñi, 2019b; Pinkwart et al., 2019). Nanodomains can be considered putative heterogeneous structures within the membrane which are due partly to phase separation.

The mechanical role of the lipid membrane in force-triggered and force-sensing mechanisms in cells is of significance and adds to the better-established role of the mechanosensitive proteins (Vogel, 2006)(Kechagia et al., 2019). Membrane conformational changes such as bending, vesiculation or tubulation are involved in cellular processes including adhesion, signaling, endocytosis or membrane resealing (van Meer & de Kroon, 2011)(van Meer et al., 2008)(Hassinger et al., 2017). For instance, in endocytosis, the endocytic system needs to generate enough force to form an endocytic vesicle by bending the membrane. These mechanisms generally require the membrane separation from the cytoskeleton as well as strong bending, for which the membrane chemical composition and physicochemical properties, often highly localized and dynamic, are key players (Sheetz, 2001)(van Meer et al., 2008). It is now clear that the lipid packing and composition are direct modulators of the membrane curvature and elasticity, at different scales, even locally at the nanometer scale (Yeagle, 1989)(Vereb et al., 2003). Understanding the lipid bilayers structural and mechanical properties and the involvement and role of each individual component turns out to be essential in order to identify their contribution to the overall membrane traits. Structural and physical properties of lipid bilayers include shape and local distribution of components (phases and domains), and related mechanical stability in response to compression, bending or stretching, their ability to fuse, etc.

We review the nanomechanics of solid-supported lipid membranes and how these relate to lipid membrane phase behavior. To this end, we chose two complementary techniques with nano/mesoscale sensitivity to mechanical and viscoelastic properties, namely quartz crystal microbalance with dissipation monitoring (QCM-D) and atomic force microscopy (AFM). QCM-D is a label-free surface-sensitive technique, whose working principle is based on the inverse piezoelectric effect. Real-time simultaneous measurements of resonant frequency and energy dissipation make QCM-D very suitable for gravimetric and viscoelastic characterization of solid-supported nanoscale sized films. AFM is a technique that allows the observation of surfaces under controlled liquid environment, to resolve topographical features with nanoscale resolution and to measure and apply forces in the pN-nN range. Therefore, AFM is appropriate for imaging the topography of solid-supported lipid membranes and probing the physical and mechanical properties at the nanoscale by means of force spectroscopy, providing high spatial and force resolution. QCM-D is complementary to AFM, useful for probing changes in viscoelastic properties during solid-supported film formation. The complementarity of AFM and QCM-D manifests at different levels: i) AFM measurements are performed at a local level, while QCM-D provides a global characterization of the solid-supported films; ii) both techniques enable dynamic mechanical analysis by applying a small oscillatory stress, however, the AFM tip scans and deforms supported layers from the top, whereas QCM-D measures the sensor oscillation from the bottom. The combination of AFM and QCM-D for supported lipid membranes has been employed in previous works (see, for instance (R. Richter et al., 2003, 2003; Van Lehn et al., 2014). In the following sections we briefly describe the membrane models and discuss the working principles behind both approaches, highlighting the quantitative and qualitative mechanical information that can be extracted using each technique. Specific examples on the usefulness to monitor phase transitions on one-component to more complex bilayers, and resolve domain coexistence are also provided, including the key role of cholesterol.

3. Experimental approaches to study membrane mechanics

3.1. Model systems: supported vesicles layers (SVLs) lipid bilayers (SLBs)

Due to the extreme complexity of biological membranes, cell membrane mimetics are excellent approaches to study membrane properties and biological processes at the cellular and subcellular level. A great deal of what we know about these processes comes from modeling lipid bilayers *in vitro*. Various membrane systems are established as biomimetic structures. They include vesicles: freely-suspended and supported liposomes, giant unilamellar vesicles (GUVs); micelles, bicelles; suspended and supported lipid films: Langmuir monolayers, phospholipid bilayers nanodiscs, black lipid membranes (BLM), supported lipid bilayers (SLB), tethered bilayer

lipid membranes (tBLM), polymer-cushioned membranes, protein-tethered bilayer lipid membranes (ptBLM) and hybrid bilayers (Sebaaly et al., 2019)(Dimova, 2019)(Doktorova et al., 2018)(Siontorou et al., 2017)(Rascol et al., 2016). Among these, the giant unilamellar vesicles (GUVs) have been extensively used since they offer a perfect stage to study the mechanical, thermodynamic, electrical, and rheological properties of the overall GUV and lipid bilayer as a function of membrane composition, surrounding media and temperature (Dimova, 2019)(Evan Evans et al., 2003)(Kahya et al., 2004). Being heterogeneous and dynamic at the nanoscale, nanotechnology-based techniques can further explore biomembranes locally with resolution at the nanometric level. For many of these techniques, like surface analytical techniques, solid-supported models are the most adequate, including supported lipid monolayers, supported vesicles layers (SVLs) or supported lipid bilayers (SLBs).

SVLs are the precursor solid-supported systems to planar SLBs formed by vesicle fusion and rupture. They result from spontaneous adsorption of small vesicles of diameter $d \leq 200$ nm onto solid surfaces. The geometry of SVLs embodies membrane curvature, tension and osmotic stress within the supported layer. This makes SVLs useful biomimetic platforms to probe membrane deformation using surface-sensitive techniques and testing ground for adhesion, budding and lipid membrane exchange and fusion (Lipowsky & Seifert, 1991; Hurley et al., 2010; Tabaei et al., 2016; Steinkühler et al., 2019). SVLs are generally formed by small soft adsorbates which are mimics to small endosomes or exosomes. These are optically inaccessible systems and the experimental investigation of their deformation is not straightforward. Adsorbed vesicles onto inorganic surfaces also serve as model systems relevant to biocompatibility studies. Vesicle adsorption is very often accompanied by vesicle deformation upon contact with the solid support. The extent of vesicle deformation depends on several factors such as vesicle size, mechanical properties of the vesicles, adhesion strength of the surface, osmotic pressure difference over the vesicle, etc. The fate of vesicles upon adsorption on a solid support depends both on vesicle-vesicle and vesicle surface interactions. In the absence of osmotic stress and at a concentration where vesicle surface coverage enhances fusion probability, the rupture of vesicles will depend strongly on the adhesion strength. Specifically on how this imbalances the energetic competition between adhesion energy and an elastic stretching of the membrane (Lipowsky & Seifert, 1991). If the adhesion strength W is large enough and exceeds the lysis tension of the membrane, the vesicles will rupture. SVLs are typically formed on surfaces whose adhesion strength is not sufficient to induce vesicle rupture, such as Au, TiO_2, Pt (Tero, 2012).

SLBs are very manageable platforms relatively simple to obtain and that retain two-dimensional order and lateral mobility. They are ideal to study lipid lateral interactions and membrane local

mechanical properties, growth of lipid domains, as well as interactions between the lipid membrane and proteins, peptides and drugs, cell signaling, etc. They also offer an excellent environment for inserting membrane proteins. There are many different methods that can be used to obtain SLBs, like the spin-coating and hydration (Mennicke & Salditt, 2002), microcontact printing (Strulson & Maurer, 2011), solvent-exchange deposition (Tabaei et al., 2016; Hohner et al., 2010), and the most widely used methods like the Langmuir–Blodgett/Schäfer deposition to prepare mono and bilayers (Kurniawan et al., 2018), and the liposome fusion and rupture method for bilayers (Hardy et al., 2013)(Mingeot-Leclercq et al., 2008). The liposome rupture method remains the most popular and simple one, based on depositing small unilamellar vesicles (SUVs) from a suspension onto a flat substrate where the adhesion strength is high, generally mica or silicon oxide, but can also be formed on bare or gold-coated glass, following the needs of the analysis technique (Mingeot-Leclercq et al., 2008; Ralf P Richter & Brisson, 2005)(Choi et al., 2016; B. Gumí-Audenis et al., 2018; Seeger et al., 2010; Winkler et al., 2020). Once in contact with the substrate the SUVs start fusing between them, deforming, flattening, and finally rupturing to form a continuous film. It is important to have in mind that the final SLB structure is affected by variables like the lipid vesicles composition, concentration, and size, the physicochemical environment pH, temperature, and ionic strength, as well as the surface roughness and charge density (Reimhult et al., 2003).

3.1 QCM-D

Quartz crystal microbalance with dissipation monitoring (QCM-D) is an acoustic-based surface-sensitive technique that enables label-free, real-time simultaneous measurements of wet-mass and viscoelastic properties of solid-supported nano/meso-scaled adlayers.

The QCM-D sensor consists of an AT-cut quartz crystal being sandwiched between two electrodes. When an AC voltage is applied across the electrodes with a frequency close to the resonant frequency of the quartz crystal, a mechanical deformation is induced, resulting in a standing shear wave. The surfaces of the electrodes coincide with the antinodes of the standing shear wave with wavelength $\lambda = 2d/n$, with d the quartz thickness and n the (odd) overtone number. The resonance frequency at each overtone is $f_n = nv/2d$, with v the speed of sound in quartz. The shear waves propagate as evanescent waves decaying across the boundary between the crystal and the fluid environment (air or liquid) with a penetration depth $\delta = \sqrt{\eta_L / \pi f_n \rho_L}$, which depends on the overtone frequency f_n and on the viscosity η_L and density ρ_L of the fluid in contact with the sensor surface (Reviakine et al., 2011). The penetration depth of a 5 MHz shear wave in water is $\delta \sim 250$ nm, rendering QCM-D surface-specific. D is defined as the ratio

between the dissipated energy during one vibration period and the total energy of the crystal at that instant $D = E_{lost} / 2\pi E_{stored}$. In the so-called 'ring-down method' measurements, energy dissipation *D* can be calculated when the AC voltage driving the quartz crystal oscillation is turned off. The working principle of QCM-D is reflected in Figure 1, upon the presence of a soft, viscoelastic layer such as a layer of lipid SVLs. The amplitude of the crystal oscillation decays exponentially and much faster when in contact with a viscoelastic layer, characterized by a large energy dissipation response.

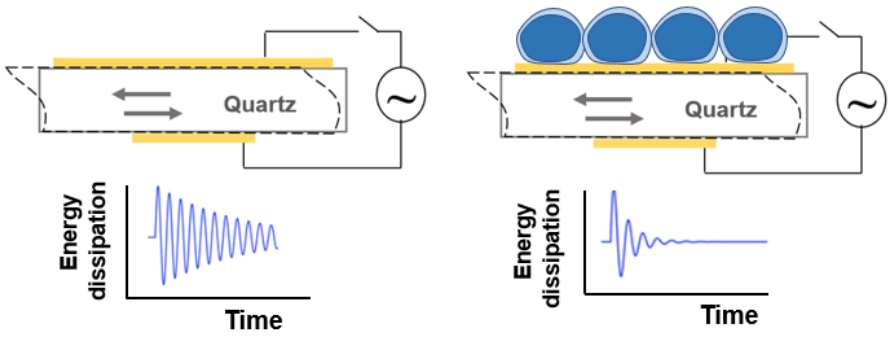

Figure 1. Schematic view of a QCM-D sensor excited by an AC voltage. Left panel: Bare Au-coated sensor in liquid environment, the dampening of the oscillations takes place slowly. Right panel: The presence of an adsorbed lipid vesicle layer (SVL) induces a faster damping of the oscillations and thus a larger energy dissipation.

Commercial QCM-D instruments allow for monitoring changes in frequency and dissipation for several overtones (n = 3, 5, 7,. . ., 13), Δf_n and ΔD_n, upon the presence of a nano/mesoscale layer. The spectroscopic data at multiple frequencies with varying detection range enables assessing the spatial homogeneity and rigidity of the adsorbed layer. For homogeneous thin and rigid films, $\Delta D_n \sim 0$, Δf_n overtones overlap and a simple relationship between mass adsorbed and change in frequency holds, the so-called Sauerbrey relation: $\Delta m = -C\Delta f / n$, with *C* being the Sauerbrey constant which for a 5 MHz quartz crystal reads $C = d\rho_{quartz} / f_0 = 17.7 ng / cm^2$ (Sauerbrey, 1959). For thicker and softer films $\Delta D_n > 0$, overtones do not overlap and the ensemble quartz-film-fluid can be represented by simple models combining elastic components and viscous dashpots. These models enable to extract effective viscoelastic parameters of the adsorbed film such as shear viscosity, thickness and shear storage modulus (Cho et al., 2007; Voinova et al., 1999).

The capability of monitoring the viscoelastic properties during film formation is particularly useful in the case of solid-SLB formation. QCM-D has been a valuable tool in deciphering the kinetic pathways of SLB formation from precursor vesicles and how those depend on relevant

conditions such as solid surface adhesion strength, medium ionic strength, vesicle mechanics, etc. (Cho et al., 2010; Jing et al., 2013; C. A. Keller & Kasemo, 1998; Pramanik et al., 2016; R P Richter, 2006).

Figure 2 shows a typical QCM-D experiment where real-time monitoring of the adsorption of zwitterionic DOPC vesicles onto SiO_2 and oxidized Au was carried out at 37 °C. The vesicles are dispersed in TRIS-buffer (10 mM TRIS, 100 mM NaCl, pH 8) at a concentration of 0.1 mg/mL and their hydrodynamic diameter d = 79 ± 20 nm. As initially discussed by Keller and Kasemo (C. A. Keller & Kasemo, 1998), the adsorption kinetics is surface-specific. The mechanistic picture of Δf and ΔD changes is governed by a delicate balance between the adhesive contribution to the free energy from lipid-surface interactions and the opposing effect of bending and stretching the membrane (Lipowsky & Seifert, 1991). DOPC vesicles adsorbing on SiO_2 follow a two-step adsorption process consisting of i) adsorption of a critical number of vesicles and ii) fusion, rupture and formation of an SLB. This is reflected in the Δf_n and ΔD_n signals depicted in the upper panels of Figure 2. After a ~ 10 min baseline in buffer (Δf_n and $\Delta D_n = 0$), DOPC vesicles added at a very small flow rate adsorb onto the SiO_2-coated quartz sensor (Δf_n decreases and ΔD_n increases) until a maximum number (minimum in Δf_n and maximum in ΔD_n). Adsorbed vesicles then fuse and rupture as a consequence of the large adhesion strength of SiO_2, thus releasing the entrapped aqueous buffer. As a consequence, Δf_n increases (mass loss) to a constant plateau of $\Delta f_n \sim -25$ Hz and the ΔD_n signal decreases back to a very small value ($\Delta D_n < 0.5 \cdot 10^{-6}$). The final Δf_n and ΔD_n values and the fact that overtones signals overlap is consistent with the formation of a homogeneous rigid and thin DOPC SLB. The pathway of SLB formation is not unique and depends strongly on the ionic conditions (head group charges of the constituent lipids, buffer ionic strength presence of divalent cations, pH). Vesicles containing positively charged lipids like DOTAP SUVs rupture individually on SiO_2 as a consequence of stronger vesicle-support electrostatic interactions (R. Richter et al., 2003).

When DOPC vesicles adsorb onto an oxidized Au surface, a monotonic Δf_n decrease and ΔD_n increase can be observed reaching constant non-zero plateau values with non-overlapping overtones. Such time-dependent responses provide evidence that oxidized Au facilitates non-ruptured vesicle adsorption towards the formation of acoustically non-rigid vesicle layers with saturated coverage. As pointed out by Lind and Cárdenas (Lind & Cárdenas, 2016), it is worth mentioning that local vesicle rupture events and formation of small bilayer patches cannot be ruled out. As a matter of fact, QCM-D is very sensitive to hydrodynamic (wet) mass and the local, partial formation of SLBs might be masked by the adsorption of vesicles on top or in between the bilayer patches. In this case, complementary QCM-D and AFM measurements are

particularly useful to obtain a complete picture of the heterogeneous layers SLBs with co-adsorbed vesicles formed. For example, the complementarity of AFM and QCM-D has proven successful in experimentally confirming defect (protrusion)-driven nanoparticle interactions with SLBs (Van Lehn et al., 2014).

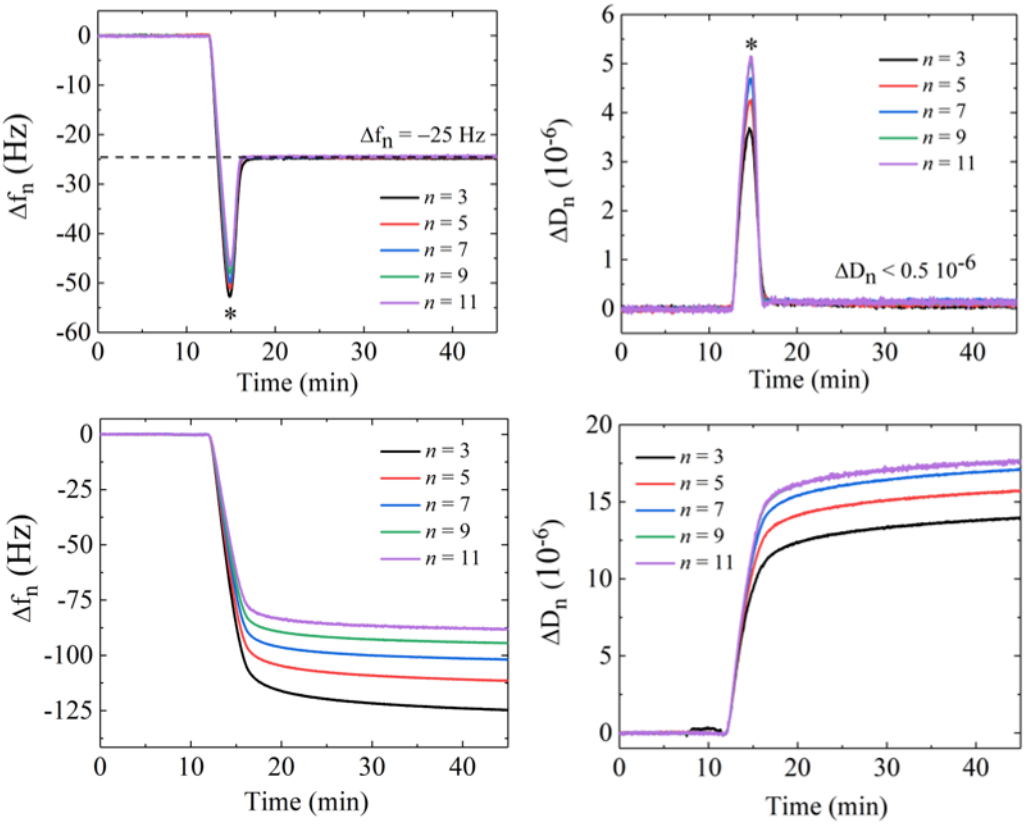

Figure 2. Time dependence of Δf_n and ΔD_n during a QCM-D experiment of DOPC vesicle adsorption at 37°C onto SiO_2 (upper panels) and Au (lower panels).

Apart from kinetic information, QCM-D can be also useful to estimate the extent of vesicle deformation upon adsorption following a model-free approach introduced by Tellechea *et al.* (Tellechea et al., 2009). This method consists in plotting $-\Delta D/\Delta f$ ratio vs $-\Delta f$ for all overtones during initial adsorption, which shows a linear decrease over a large range of frequency shifts. Extrapolation of this linear decrease to a frequency-independent intercept with the $-\Delta f$ axis (where overtones intersect) provides a value of the thickness of the adsorbed vesicle layer h or Sauerbrey thickness: $h = -\Delta f\, C / \rho$, where C = 17.7 ng/cm^2 Hz and ρ = 1 g/cm^3 is the density of the film. This approach assumes a complete surface coverage, where the presence of trapped buffer has been diminished to occupy only the void spaces between densely packed vesicles (the $-\Delta D/\Delta f$ ratio is close to zero and the $-\Delta f$ intercept values were the same on the extrapolation of a linear regression) (Tellechea et al., 2009; Reviakine et al., 2012; Olsson et al., 2013). Figure 3

displays the extrapolated Sauerbrey thickness for DOPC SUVs adsorbed onto SiO_2 and Au surfaces. The respective effective frequencies read h(SiO_2) = 30 ± 2 nm and h(Au) = 62± 5 nm. If one compares these values with the original vesicle diameter in bulk measured by DLS (d =79 ± 20 nm), vesicles were deformed to a greater extent onto SiO_2 surfaces. A more exact approach based on a hydrodynamic model was recently introduced by Cho and co-workers (Gillissen et al., 2017) to estimate the deformation of small vesicles at low surface coverage. The model enables to estimate adsorbed vesicle shape and bending energy by using hydrodynamic spectroscopy (frequency shifts at several overtones). It treats vesicles as ellipsoids and relates the so-called QCM-D force to the scaled viscous penetration depth δ/a with δ the viscous penetration depth, and a the non-deformed vesicle radius, in order to probe the adsorbed particle aspect ratio. Further details on the model can be found in (Gillissen et al., 2017).

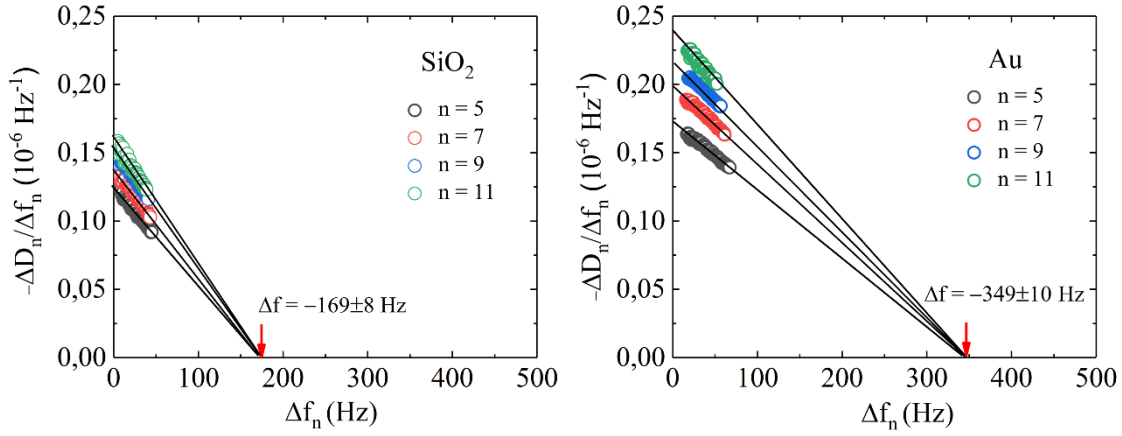

Figure 3. $\Delta D_n/-\Delta f_n$ ratio as a function of frequency at different overtones for DOPC vesicles adsorbed onto SiO_2 and Au.

3.2. Atomic Force Microscopy (AFM)-based methodology

Classical structural techniques such as X-ray, NMR or electron microscopy rely on ensemble averaging of molecular properties. Yet, by these means, the underlying molecular dynamics can be hidden, since the signal comes from the average of many unsynchronized molecules in the bulk. The picture changes when using single-molecule techniques. The measured signal of one - or a few- molecules reflects the stochasticity of thermally induced processes when randomly crossing free-energy barriers. Single-molecule optical microscopy techniques are particularly well suited for the study of the dynamics of molecules. However, these latter methods rely on the detection of fluorescent markers attached to proteins or lipids, which means that the resolution is limited to ~200 nm due to diffraction of light and to a few tens of nm thanks to super-resolution techniques. The atomic force microscopy (AFM) was since its invention in 1986 (Binnig et al., 1986) quickly positioned among the single-molecule, high-resolution structural

analysis techniques. It provides information concerning structure, function-related conformational changes and supramolecular assemblies, crucial for a complete understanding of biological processes. Nowadays, AFM is in its thirties and has become an invaluable tool for studies at the micro- and nanoscale. As a stand-alone, high-resolution imaging technique and force transducer, it is today an established methodology among the biophysical community. The AFM uses a nanometer-sharp tip -resembling a record player needle- attached to a (micro)cantilever to sense the sample surface while scanning it using piezoelectric elements. An optical system is used to detect the cantilever deflection (or force), thanks to a laser diode beam reflected on the back of the cantilever and detected by a photodiode. Changes in deflection due to sample protrusions while the tip scans the sample are translated into electrical signals thanks to a feedback mechanism. This is schematically represented in Figure 4.

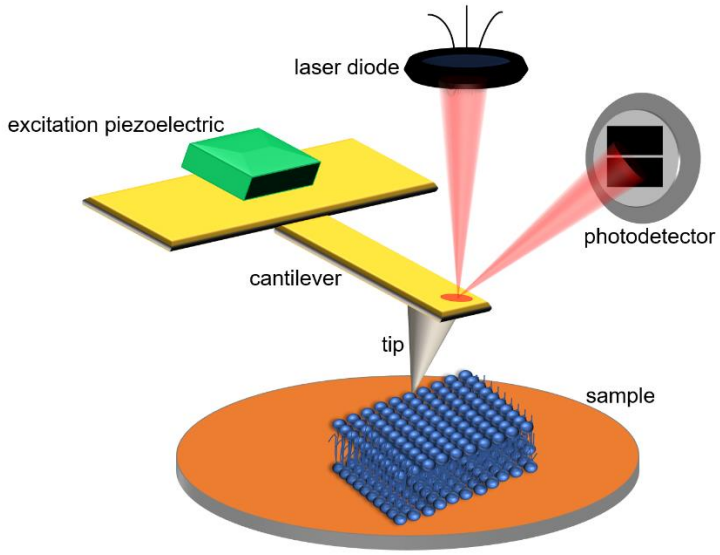

Figure 4. Schematic representation of an AFM instrument. The deflection of the cantilever in the normal direction is monitored by a photodetector which collects the reflection of a laser beam focused at the back of the AFM cantilever. In the tapping mode, thanks to a piezoactuator, the AFM cantilever is excited near its resonance frequency.

One of the main strengths of AFM relies on the possibility of working in a controlled environment (medium composition and temperature) and with great spatial resolution. AFM-imaging mode provides submolecular resolution on a large variety of biological samples: from single molecules, that is, DNA or proteins, to supramolecular assemblies such as SLBs, or even entire cells (Giles et al., 1993)(Dufrêne et al., 2017; Parot et al., 2007). Therefore, AFM has become a well-established technique for imaging the topography of lipid membranes that show homogeneous or phase-separated morphology, permitting then to increase the bilayer complexity, from

bilayers of one component to multicomponent ones (El Kirat et al., 2010; B. Gumí-Audenis et al., 2016a; Morandat et al., 2013; L Redondo-Morata et al., 2014).

For the study of biological samples, it is common to use AFM-imaging dynamic modes that have an intermittent tip-sample contact. Among them, the most often used is oscillation or tapping mode, in which the AFM cantilever is excited near its resonance frequency. The resulting oscillating tip is intermittently contacting -tapping- the surface, giving rise to a damped oscillation amplitude. Additionally, the resonance frequency is also shifted due to the probe-surface interaction. The topography of the surface is reconstructed by monitoring the amplitude of the oscillating cantilever, which is kept constant by adjusting the z-piezo position through a feedback loop. While scanning in the X-Y direction, the amplitude of the cantilever oscillation is kept constant thanks to a feedback control. However, biomolecules are dynamic in essence; hence, to understand how biomolecules work it was only natural to think about increasing the temporal resolution of conventional AFMs. The first time that the concept of High-Speed (HS) AFM was mentioned -to our knowledge- was in 1991 by Barrett and Quate (Barrett, 1991), who did a fairly attempt with the technology at that time. Other research groups, as Paul Hansma's, would challenge the practical speed limitations. It was only in 2010 when the laboratory leaded by Toshio Ando in Kanazawa University (Japan), filmed individual myosin molecules walking on an actin filament (T Ando et al., 2008), operating their AFM instrument at a speed about 1000 times faster than the conventional instruments of that time. Besides the visual impact and scientific insight of those movies, these experiments illustrated that HS-AFM could obtain concomitantly structural and dynamic data, providing insights inaccessible by any other method (Toshio Ando, 2017; Chiaruttini et al., 2015; Kodera et al., 2010; Mierzwa et al., 2017). The basic principles, advantages and limitations of the most common AFM bioimaging mode are nicely detailed in a recent review from Dufrêne *et al*. (Dufrêne et al., 2017).

Following the capability of the AFM for mechanical manipulation, to sense and apply small forces accurately (pN-nN range), it rapidly developed into an excellent technique to study interactions -inter and intramolecular forces- at the molecular level, the so-called AFM-based force spectroscopy (AFM-FS). The manipulation of single molecules (single molecule force spectroscopy) has led to fascinating new insights in the mechanics of proteins, polysaccharides, synthetic polymers, and DNA at the molecular level (Florin et al., 1994)(Lee et al., 1994)(Radmacher, 1997)(Noy et al., 1997)(Clausen-Schaumann et al., 2000)(Rief et al., 1997)(Hugel & Seitz, 2001)(P E Marszalek et al., 1999; Piotr E Marszalek et al., 2001)(Giannotti & Vancso, 2007).

In the case of lipid bilayers, AFM offers the unique opportunity to probe local physical and mechanical properties, determining the interaction forces with nanoscale lateral resolution, thereby providing new insights into membrane molecular mechanisms. For the nanomechanical characterization with AFM, an SLB is generally first imaged and then a series of force-distance curves is recorded over the same area. In each force-distance curve, the AFM tip away from the surface is approached and retracted at constant velocity while the cantilever deflection is recorded as a function of the Z piezo position. Each portion of the force-distance curve provides information about the physical and mechanical properties of the bilayer, schematized in Figure 5. Upon mechanical contact during approach, the cantilever deflection increases and the SLB is elastically compressed by the AFM probe until the tip suddenly breaks through the SLB, jumping into a contact with the substrate (Figure 5, b). The first part of the curve, corresponding to small elastic deformation upon compression, can be used to estimate elastic descriptors of the membrane, like the Young modulus (E), the area compression-expansion modulus (K_A) and bending modulus (k_C) (Dufrêne & Lee, 2000; Picas et al., 2012; L Redondo-Morata et al., 2016). When performing very small elastic deformations (far from the bilayer rupture) it is also often used for this calculation the retraction part of the curve. To estimate the elasticity of the lipid film, the most common model used is the Hertz model, where the surface is approximate to an infinitely half-space of an isotropic elastic solid and the indenter as non-deformable. The parameter describing the sample is the Poisson's ratio (v), which depends on the nature of the material. For soft biological samples, the Poisson's ratio is generally set to 0.5 (as for incompressible materials). The geometry of the indenter determines the contact area. The original Hertz model considers the shallow contact between two spherical bodies, but several extensions were made for different indenter geometries (D. C. Lin et al., 2007). Again, when performing experiments with small deformations far from the onset of the lipid bilayer rupture, the hysteresis found between the approach and the retract curves is considered as dissipation work and can be used to obtain intrinsic viscoelastic parameters of the viscoelastic material, by the adaptation of common viscoelastic models as power-law rheology or the Kelvin-Voigt model (Garcia et al., 2020).

Moreover, different types of short-range interactions can be measured -DLVO, hydration or steric forces-, for further information review here (Lorena Redondo-Morata et al., 2012).

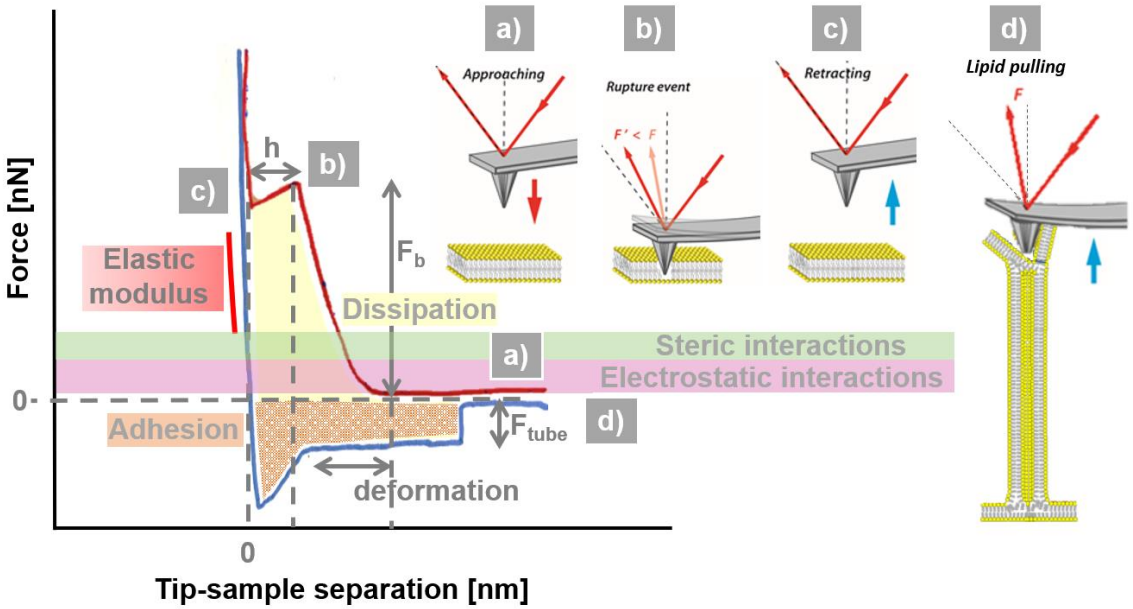

Figure 5. Schematic representation of a representative force curve typically plot in vertical force vs. tip-sample separation. The red curve represents the tip approaching (a). Right after the contact area, short-range tip-sample interactions from different nature appear, predominantly electrostatic (highlighted in pink) and steric (highlighted in green) interactions. When keeping the tip velocity constant, elastic deformation of the membrane is followed by a sudden jump (b) which is interpreted as the breakthrough force (F_b) or the maximum force the bilayer is able to withstand before breaking. F_b has been extensively used as a hallmark of the bilayer stability, some of these related works are reviewed in this chapter. The AFM tip reaching the hard substrate underneath is represented as a vertical in the force-separation curve. From the distance in the curve between the breakthrough force and the substrate it can be estimated the minimal bilayer thickness (h) (fully compressed). Afterwards, tip retracts at constant velocity (c). Elastic modulus is usually estimated from the slope of the curve which displays membrane deformation. It is often observed a hysteresis between the approach and retract curves (yellow area) which is related to dissipation work and therefore to the viscoelasticity of the material. During retraction, negative force values are used to estimate the adhesion work between the sample and the AFM tip. Sometimes, a force plateau when retracting the AFM tip away from the SLB can be observed. It characterizes a tube pulling process (c'), defined by the tube growing force (F_{tube}) until eventually the AFM tip completely detaches.

The penetration of the AFM tip through the bilayer appears as a discontinuity in the approaching force-separation curve (Figure 5, b). The vertical force at which this discontinuity happens corresponds to the maximum force the bilayer is able to stand before breaking and is defined as the breakthrough force (F_b) or yield threshold force, first observed in the end of the 90's by

437 Dufrêne et al. (Dufrene et al., 1997, 1998)(Dufrêne & Lee, 2000; S Garcia-Manyes & Sanz, 2010;
438 B. Gumí-Audenis et al., 2016a; L. Redondo-Morata et al., 2012; Schneider et al., 2000). F_b is
439 generally of several nanonewtons (nN) and it is considered as a direct measurement of the
440 lateral interactions within the lipid bilayer, at a specified loading rate. From the step in the
441 separation before and after the breakthrough, the SLB thickness at different compression forces
442 (and at zero force) can be extracted.

443 The mechanical rupture of lipid bilayers is of thermal fluctuation nature, whose destructive
444 action is facilitated and directed by the application of the external force. The penetration of the
445 AFM tip through the SLB has been modeled and conceived as a two-state process with an
446 associated energy barrier (Butt & Franz, 2002; Franz et al., 2002; Simona Loi et al., 2002).
447 Specifically, two models describe the activation process. The first is the continuum nucleation
448 model, which considers the bilayer as a molecular thin homogeneous film -a two-dimensional
449 fluid layer- between the solid substrate and the solid surface of the AFM tip. The second model
450 ponders the molecular nature of the lipid bilayer and proposes that each molecule in the SLB
451 has specific binding sites corresponding to energetically favorable positions. These sites are
452 energetically equivalent, and as the SLB is pressed by the AFM tip, the energy of the molecules
453 significantly increases, leading them to jump apart and create a hole under the tip. After a critical
454 number of molecules have jumped out of the contact area, the tip indents the SLB due to the
455 high pressure of the remaining molecules, breaking the bilayer. Determining the energy barriers,
456 represented by the Arrhenius law, governing the lipid membranes rupture process contributes
457 to the understanding of the extent of the lateral interactions in the bilayer, and this is generally
458 achieved by following the variation of the F_b with the loading rate (r) by varying the tip-sample
459 approaching velocity (v) in what is called the dynamic force spectroscopy (DFS). Out of
460 equilibrium, the F_b increases linearly with the logarithm of r (and of v as well) (Butt & Franz,
461 2002; S Loi et al., 2002). The loading rate dependence with the thermomechanically activated
462 nature of the bilayer rupture kinetics leads to the evaluation of the activation energy of the
463 bilayer failure in the absence of an external force (ΔE_0). The activation energy ΔE for the
464 formation of a hole in the bilayer that is large enough to initiate rupture and lead the tip
465 breakthrough can then be calculated following the expression proposed by Butt et al.:

$$\Delta E(F_b) = -k_B \cdot T \cdot ln\left[\left(\frac{0.693 \cdot k_S}{A}\right) \cdot \frac{dv}{dF_b}\right] \quad \text{(Eq. 1)}$$

466 where k_B is the Boltzmann factor, T is the absolute temperature, k_s is the cantilever spring
467 constant, A is the frequency at which the AFM tip attempts to penetrate the bilayer, generally

approximated to the resonance frequency of the cantilever, v is the tip velocity, and F_b the breakthrough force.

When retracting the AFM tip away from the SLB, it sometimes remains connected to the bilayer through a lipid tube (Figure 5, d). While the tip moves further away, the membrane tube grows longer until it breaks at a certain distance, and the cantilever returns to the equilibrium position. This tube pulling process occurs at constant force, the tube growing force (F_{tube}) (Armond et al., 2011; Berta Gumí-Audenis et al., 2018; Maeda et al., 2002; Ralf P Richter & Brisson, 2003), and it is observed as a force plateau in the retract part of the force-separation curve (Figure 5), at several tens of pN from which F_{tube} and the tube growing distance (d) can be recorded. Pulling lipid tubes with an AFM tip out of SLBs is a simplified but analogous situation to some biological processes involving mechanical and conformational adjustments -bending, vesiculation, tubulation-like formation of membrane tethers, endocytic vesicles, etc. (Schmidtke & Diamond, 2000; Shao et al., 1998; Sheetz, 2001; van Meer et al., 2008). Separation of a membrane segment from the cytoskeleton as well as strong membrane bending are both involved, for which the membrane chemical composition and physicochemical properties are key players. Pulling tethers from cells with an AFM probe is a widely explored approach to evaluate the membrane mechanics on entire cells (Brochard-Wyart et al., 2006; Marcus & Hochmuth, 2002; Nawaz et al., 2015; Sun et al., 2005). Recently, it has also been established as a method to locally probe SLB mechanics and the contribution of the underlying substrate to the measured properties on SLBs (Berta Gumí-Audenis et al., 2018).

When pulling tethers from cells, the F_{tube} depends on the membrane properties like bending stiffness (k_c) and in-plane membrane tension (σ), and also on the adhesion between the membrane and the cytoskeleton (Sheetz, 2001). In regions where the membrane has separated from the cytoskeleton -bleb or free membrane-, as there is no direct interaction with the cytoskeleton, F_{tube} strictly relies on k_c and σ (Dai & Sheetz, 1999). However, the cytoskeleton adhesion and σ are difficult terms to separate, and therefore the concept of apparent membrane tension, σ_{app}, has been proposed to include the adhesion energy parameter γ (Sheetz, 2001), $\sigma_{app} = \sigma + \gamma$. When the lipid tube grows under thermodynamic equilibrium, at the limit of zero velocity (static thermodynamic analysis), the following mathematical expression relates the membrane parameters mentioned above with the F_{tube} (Armond et al., 2011; Canham, 1970; Daillant et al., 2005; E Evans & Yeung, 1994; Berta Gumí-Audenis et al., 2018; Hochmuth et al., 1996; Marcus & Hochmuth, 2002; Roux, 2013): $\sigma_{app} = \frac{{F_{tube}}^2}{8k_c\pi^2}$.

The plus of this approach, AFM-based pulling lipid tubes from SLBs, is that it combines the advantage of the AFM local probing with nanoscale lateral and force resolution, with the simplicity of the SLB model preparation. Besides, the local nanomechanical properties of SLBs can be explored through the combination of the tubing force spectroscopy approach and the F_b analysis exposed before, within the same experimental procedure (Berta Gumí-Audenis et al., 2018).

Although it will not be extensively discussed here, we find important to mention that the constant force approach can also be used to evaluate the membrane rupture kinetics in SLBs and supported lipid multibilayers (SLMs). The AFM tip is approached at constant velocity, and then compresses the membrane at a constant force (force clamp, FC). Through measuring the time it takes to penetrate the bilayer -time to breakthrough (t_b)- distribution at different compression forces, the AFM-FC mode allows to estimate the rate of bilayer failure and calculate the location of the energy barrier maximum -distance to the transition state- along the reaction coordinate (Δx) and the activation energy (E_0) that characterize the energy barrier (L Redondo-Morata et al., 2012a; Relat-Goberna et al., 2017). Both E_0 as well as Δx were found to be higher for SLBs than for supported lipid multibilayers, endorsing previous suspicion that the mechanical properties of lipid bilayers obtained from nano-indentation are strongly influenced by the underlying hard substrate.

4. Phase behavior and nanomechanics. From one component membranes to higher complexity

4.1. One-component membranes

4.1.1. The gel and the fluid phase

To start with the simplest system and increase the complexity in this revision -which does not intend to be exhaustive- consider a one-component phospholipid bilayer, which is thermalized at a temperature far from its T_m, the temperature of the main phase transition, at which a disordering of the hydrophobic tails happens followed by a sudden increase of the lateral mobility. We are then able to distinct two different main phases, gel-like or solid ordered phase (s_o) below T_m, and fluid-like phase or liquid disordered (l_d) above T_m.

A mechanical descriptor of lipid bilayers that shows significant differences between both phases is the bending modulus k_c. At $T < T_m$, k_c is an order of magnitude larger than at $T > T_m$, rendering lipid vesicles quite stiff, while softer and more deformable above T_m. In the case of SVLs, where probing deformation is not straightforward, QCM-D has proved to be a useful tool to estimate the extent of vesicle deformation upon adsorption onto surfaces. Reviakine and co-workers

(Reviakine et al., 2012) reported deformation measurements of small DMPC vesicles on TiO_2 above and below T_m, and experimentally found out that adsorbed vesicle deformation correlates with the bilayer bending modulus. Liposomes in the fluid phase bear a smaller bending modulus and deform to a greater extent.

When imaged with the AFM, the SLBs show typically 4-6 nm of height. The measured height is also influenced by both the elasticity of each bilayer and the particular AFM methodology, *i.e.* acoustic-modulation "tapping" mode, contact mode, etc, where the representation of the interface of the lipid bilayer changes. In terms of its mechanical properties, whether we are measuring the elastic deformation or the yield threshold force, a one-component SLB yields a monomodal distribution. While the distribution of deformations or breakthrough forces of the bilayer, being a stochastic process, have been often approached to Gaussian distributions, other distributions based on different theoretical frameworks can also be found in the literature, like the models proposed by Franz *et al*. (Butt & Franz, 2002) for the two-state activation process of the bilayer rupture, mentioned in section 3.2.

In the first place, it could be said that, in a general way, the bilayer thickness depends on the nature of the lipids -solid-like bilayers are usually higher than liquid-like counterparts of similar number of carbons in the hydrocarbon chains. In an s_o phase, the hydrocarbon chains are stretched, so the apparent height is greater, and this is observed when imaging SLBs by AFM. Consequently, stretched acyl chains lead to stronger van der Waals interactions between neighboring molecules, which translates into a shorter intermolecular distance between phospholipids, and a greater mechanical resilience, both elastically and upon AFM tip penetration.

For example, let's briefly consider the elastic deformation of DOPC and DPPC, as models of l_d and s_o SLBs, respectively. The slope of the curve in the contact zone (elastic regime), as we have commented in section 3.2, is related to the elastic modulus of the material. At room temperature, the slope for the DOPC SLB, which is in the fluid phase, is lower than that for the solid DPPC SLB. This indicates that DPPC bears a larger Young modulus than DOPC and thus the membranes in the s_o phase are therefore stiffer than in the l_d phase. Both slopes are smaller than the one that can be measured on the bare substrate (often assumed as an infinitely stiff material, such as mica).

Besides the evidenced difference in elasticity for the fluid and gel-like membranes, l_d SLBs show in general lower F_b values than s_o SLBs. A good example are homologous series phospholipids; while at room temperature DLPC ($T_m \sim -2$ °C) SLBs break at force values between 2 and 13 nN,

according to the ionic environment, DPPC (T_m ~ 41.5 °C) SLBs are pierced by the AFM probe, in similar conditions, in the force range that goes from 7 to 30 nN (Lorena Redondo-Morata et al., 2012). It is also noticeable that the F_b increase with the logarithm of the loading rate is lower for the fluid than for the gel membranes (Lorena Redondo-Morata et al., 2012). This can be expected, if we consider the Bell-Evans or assimilable model, the most likely breaking force depends linearly on the logarithm of the loading rate r, $F(r) = \left(\frac{k_B T}{x}\right) \ln \frac{rx}{K_0 k_{BT}}$, where k_B is the Boltzmann constant, x is the distance to the transition state and K_0 is the off-rate constant at 0 force (E Evans & Ritchie, 1997). In this case, x is directly related to the distance between neighboring phospholipid molecules. This intermolecular distance, therefore x, is smaller in s_o than in l_d.

Early work showed how AFM-FS is able to explore quantitatively the molecular determinants that provide mechanical stability to the supported membrane (S Garcia-Manyes, Oncins, et al., 2005a; Sergi Garcia-Manyes et al., 2010). By systematically and independently changing the chemical composition of the lipid headgroup, the length of the hydrophobic tail, and the number of chain unsaturations,{Citation} it was possible to describe the mechanical stability of each bilayer as a direct signature of membrane lateral organization (S Garcia-Manyes et al., 2010). The distribution of F_b values as a function of the length of the hydrophobic chain showed that on average, increasing each hydrocarbon tail by 2 extra –CH_2– groups results in ~ 7 nN increase of the F_b, equivalent to an enthalpy increase by roughly 2 kJ/mol (Berg et al., 2002). In the same study, the mechanical properties of the linear DPPC were compared with its analogous branched phospholipid, DPhPC, to investigate the effect of acyl chain branching. The distribution of F_b showed a decrease from ~20 nN to ~12 nN, revealing an important contribution of the lateral -CH_3 groups on the molecular packing of the bilayer. This observation can be rationalized in terms of the larger area per lipid for the branched DPhPC (76.8 Å^2) compared to that for the linear DPPC (62.0 Å^2), as revealed by molecular dynamics simulations conducted in the fluid phase (Shinoda et al., 2007). The nanomechanical effect of the –cis double bonds present in the acyl chains was also investigated. The F_b values distributions for each particular bilayer showed an inversely proportional trend between mechanical stability and number of unsaturations. It was estimated that upon introduction of one additional unsaturation in each acyl chain, F_b values decrease by ~5 nN. Interestingly, introducing an asymmetric unsaturation resulted in an even further mechanical destabilization. The resulting molecular tilt reduces the effective packing between molecules, giving rise to a lower T_m (Berg et al., 2002). The findings regarding the mechanical implications of the headgroup chemistry were, however, far less straightforward and highly unanticipated. Comparing phospholipids with the same hydrocarbon tails but

different headgroups, a huge range of forces required to indent the bilayer in the same experimental conditions, spanning from ~3 nN (DPPA) all the way up to ~66 nN (DPPG).

Furthermore, the lateral packing differences observed between fluid and gel-like bilayers is also reflected in the tube growing force, pulled as the AFM probe moves away from the SLBs, as this approach has demonstrated to be sensible to the membrane chemical composition in one-component SLBs (Maeda et al., 2002)(Berta Gumí-Audenis et al., 2018). Higher F_{tube} values for DPPC with respect to DMPC have already been observed by Maeda *et al*. (Maeda et al., 2002) and, as reported in Gumí-Audenis *et al*. (Berta Gumí-Audenis et al., 2018), F_{tube} is lower for l_d mica-SLBs (in the range of 65–80 pN) than for s_o bilayers of the same headgroup (in the range of 90–110 pN) (Figure 6a). Additionally, while in the l_d state the F_{tube} slightly augments from PE to PC (66 ± 15 pN for DOPE, 80 ± 25 pN for DOPC and 75 ± 13 pN for DOPG), it clearly increases when changing the headgroup for s_o membranes from PE to PC and then PG (92 ± 20 pN for DPPE, 104 ± 30 pN for DPPC and 112 ± 30 pN for DPPG). Hence, F_{tube} is generally higher for s_o than for l_d and goes along with the lateral packing associated to different phospholipid headgroups, in a way that is comparable to the trend observed on the F_b approach, as can be seen in Figure 6b.

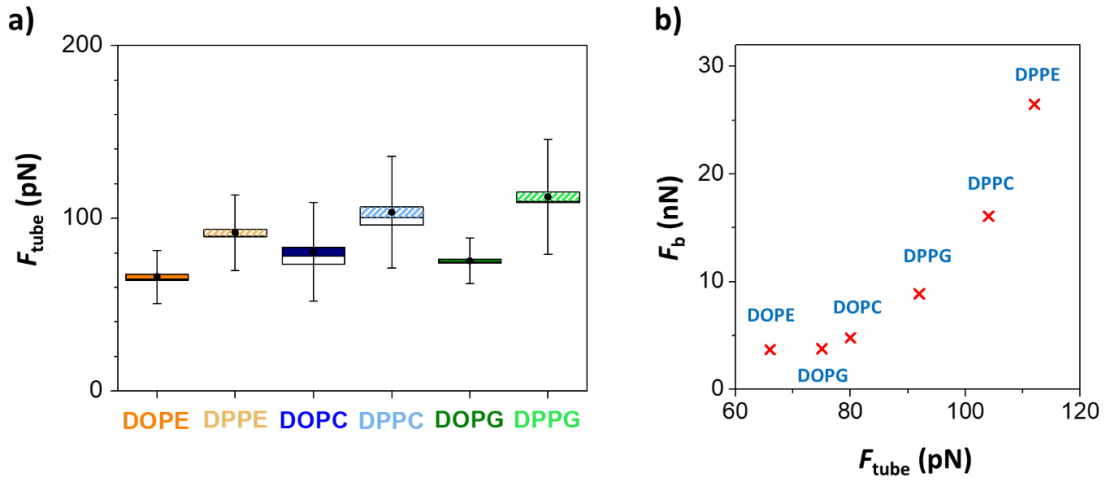

Figure 6. AFM-pulling lipid tubes sensible to the membrane composition in one-component SLBs. a) F_{tube} values for single component SLBs of different composition (DOPE, DPPE, DOPC, DPPC, DOPG and DPPG). Boxchart for F_{tube} values show the mean (●), SE (box) and SD (bars). b) Correlation between F_b and F_{tube} values for single component SLBs. The individual phospholipids contain a constant tail length of 18 C with 1 unsaturation (DOPE, DOPG and DOPC) or 16 C and fully saturated (DPPE, DPPC and DPPG), in fluid and gel state at room temperature (RT), respectively. All the measurements were performed in 150 mM NaCl, 20 mM $MgCl_2$, 20 mM

HEPES (pH 7.4) buffer solution and at RT. Adapted from Ref. (Berta Gumí-Audenis et al., 2018) with permission from the Royal Society of Chemistry.

Taken together, force spectroscopy experiments on SLBs are in qualitative agreement with the literature that correlates the physicochemical properties of membranes with the chemical composition of their phospholipid hydrophobic chains (Rawicz et al., 2000). Noteworthy, thermodynamic quantities such as the melting temperature or the order parameter can be translated into the realm of mechanical stability. The order parameter is usually calculated from NMR-based measurements and provides information about the overall membrane order and more particularly the conformations that the atoms within the lipid tails adopt (Piggot et al., 2017).

4.1.2. The thermal transition

4.1.2.1. Main transition

A useful application of QCM-D is the detection of thermotropic phase transitions within SLBs and SVLs, with the asset that it is label-free, it does not require long temperature equilibration times nor a large amount of sample. When temperature is varied in the absence of any transition, Δf and ΔD typically show a regular, linear temperature dependence, as a reflection of regular, temperature-dependent changes of the viscosity and density of the surrounding liquid medium. When approaching the main phase transition temperature, both frequency and the dissipation responses will differ from a regular temperature dependence, displaying anomalies that reveal that structural changes are taking place (Losada-Pérez et al., 2014; Neupane et al., 2018). Figure 7 displays changes in the frequency and its derivative of an SVL of DMPC of vesicles of around 130 nm, with main transition temperature $T_m \sim 24$ °C in a rather narrow temperature range. The shape of frequency shift curves and its respective temperature derivative are reminiscent of the enthalpy jump and its heat capacity derivative typically obtained from calorimetric measurements (Heimburg, 1998; Losada-Pérez et al., 2014). Dissipation typically shows jumps and minima in the same temperature range. Therefore, extrema in the first-order derivative of frequency and dissipation curves stand as a token of the layer thermotropic phase transitions. Calorimetry is a state-of-the art technique for the detection of phase transitions based on changes in thermal properties when lipids undergo the main (first-order) transition (heat absorption or release), while QCM-D is based on changes in viscoelastic properties of the adsorbed vesicles as a result of changes in bilayer thickness, rigidity and vesicle shape. Although also detectable in SLBs, the size of the jumps in Δf and ΔD is several orders of magnitude smaller than the size of the jumps observed for SVLs (Wargenau & Tufenkji, 2014; Hasan & Mechler, 2015).

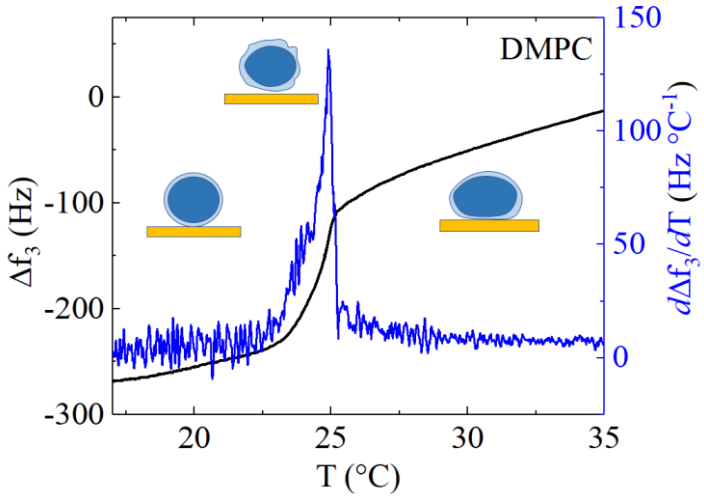

658

659 **Figure 7**. Temperature dependence of the frequency shift dΔf_3/dT (black solid line) and its first-
660 order derivative (blue solid line) of a DMPC SVL upon heating at 0.2 °C/min.

661 Reviakine and coworkers provided a comprehensive interpretation of the mechanisms by which
662 QCM-D detects phase transitions in lipid membranes and the related relative contribution of
663 thickness, stiffness and hydrodynamic channels to the Δf and ΔD fingerprints (Peschel et al.,
664 2016). Upon heating, lipid bilayers in both SVLs and SLBs change from a thicker and stiffer s_o
665 phase to a thinner and less stiff l_d one. Both stiffness and thickness changes in the lipid layer
666 properties across the transition encompass changes in the Δf signal (decrease upon heating). In
667 the case of the ΔD, the stiffness and the thickness contributions oppose each other since stiffer
668 layers dissipate less. In the SLBs, this leads to an overtone dependence of the transition peak
669 (Peschel et al., 2016). In thicker and softer SVLs, changes in the shape of the adsorbed vesicles
670 might induce further hydrodynamic channels that contribute to ΔD. As a consequence, the size
671 of the maximum in SVLs is several orders of magnitude larger than the one observed in SLBs.

672 The thermotropic phase behavior of pure SLBs has been widely related with the
673 (nano)mechanical properties of the bilayer. Combining the previously exposed approaches, the
674 AFM-FS sensitivity to the lipid phase of SLBs is evidenced, positioning it as an appropriate tool
675 to determine the phase thermal transitions. Temperature controlled-AFM has been established
676 as a suitable tool to analyze both the topographical and mechanical evolution of biologically
677 relevant issues that are temperature dependent at the nanometer scale.

678 Seminal work of Leonenko *et al*. demonstrated the existence of several phase transitions in DPPC
679 and DOPC mica-supported bilayers (Z. V. Leonenko et al., 2004). Data of both topographical
680 imaging and force measurements provide invaluable insight into membrane behavior during
681 phase transitions. For DPPC SLBs, F_b values decrease as temperature increases, and beyond the

main transition, DPPC shows similar force plots as the fluid-phase DOPC bilayers. This dependence of the F_b on the phase state of the SLB below and above T_m has been further reported for different lipids, like DMPC (T_m ~ 24 °C) that changes F_b from 13-14 nN at 20 °C below T_m to about 6 nN at or 40 °C DPPC (T_m ~ 42 °C) that shows a switch of F_b from around 20-25 nN at 27 °C to around 3-5 nN at 55 °C (S Garcia-Manyes, Guell, et al., 2005; L Redondo-Morata et al., 2012b). When the DPPC SLB is maintained a temperature slightly above T_m, coexistence of the gel and fluid phase occurs and a bimodal F_b distribution is obtained (Figure 8), as reported in Gumí-Audenis *et al*. (B. Gumí-Audenis et al., 2016a). This is because the thermal transitions in SLBs generally happen at temperatures slightly higher and in a broader range than in vesicle suspensions as a consequence of the underlying substrate affecting lateral order and interleaflet coupling (S Garcia-Manyes, Guell, et al., 2005; Z. V Leonenko et al., 2004; L Redondo-Morata et al., 2012b; Seeger et al., 2010). In Garcia-Manyes *et al*. it was shown that the main phase transition occurs in a range of temperatures of *ca*. 10-13 °C (S Garcia-Manyes, Oncins, et al., 2005b).

There is an effect of temperature on the mechanical stability for the SLBs because the increase of temperature directly affects the molecules fluctuations provoking an increment in the area per molecule -lower packing density-, especially noticeable in the gel phase, with the consequent decrease of the F_b values. At temperatures around the T_m of the lipid, and for a temperature range of a few °C, a pronounced drop in F_b takes please, as the SLB gradually transitions to the fluid phase, thereby softening. Several degrees over the T_m, the F_b values are on the order of the ones typically observed for l_d SLBs at room temperature (Alessandrini & Facci, 2012; S Garcia-Manyes, Oncins, et al., 2005a; L Redondo-Morata et al., 2012b). This can be seen in the example shown in Figure 8d, where the DPPC mica-SLB shows an F_b value around of 21 nN at 27 °C and slight decreases with temperature as the 42−45 °C range is reached. At higher temperatures, the F_b remains approximately constant at *ca*. 3.5 nN. The F_b-temperature trend displays a break around the T_m value of DPPC.

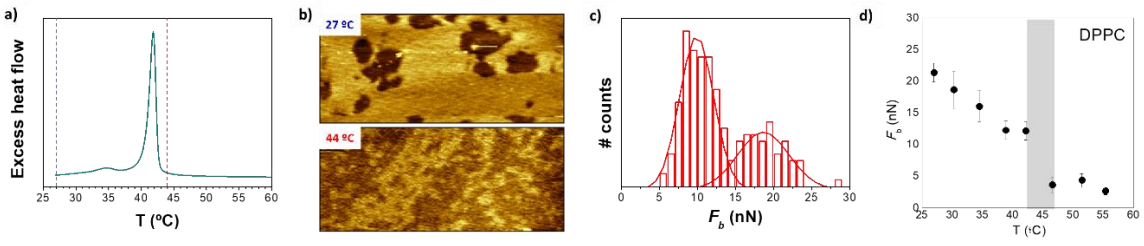

Figure 8. Phase transition of DPPC bilayers: a) DSC thermogram of DPPC vesicle suspension; b) 6 µm x 2.5 µm AFM images of DPPC silicon-SLB at 27 ºC and 44 ºC; c) F_b histogram at 44 ºC and

gaussian fits to the bimodal distribution. All experiments performed in 150 mM NaCl, 20 mM $MgCl_2$, 20 mM HEPES (pH 7.4) buffer solution. Adapted from Ref. (B. Gumí-Audenis et al., 2016a). d) Mean F_b value of DPPC mica-SLB as a function of temperature, in 10 mM HEPES, 20 mM $MgCl_2$ and 150 mM NaCl (pH 7.4). The shadowed vertical line marks the observed transition temperature range. Adapted from Ref. (L Redondo-Morata et al., 2012b)

Additionally, Mouritsen and coworkers proposed that AFM topography at a varying temperature could decouple the phase transition of the two different leaflets of the mica-supported bilayer (D. Keller et al., 2005). The low temperature transition was proposed to be related to the melting of the leaflet far from the substrate surface, and the second transition to the phase transition of the leaflet in contact with the mica. Such decoupling would respond to the stronger interaction between the lipid headgroups of the proximal monolayer and the mica support.

4.1.2.2. Pretransition

Some lipids present a pretransition before the main first-order transition which gives rise to an intermediate order in the lipid bilayers referred to as ripple phase. Ripple phases are curved structures with undulating surface topography. AFM imaging revealed the structure of the ripple phase in hydrated conditions at the nanometer scale (Kaasgaard et al., 2003), and such particular structure has been recently explored nanomechanically (Majewska et al., 2020). It can be found when solid phase lipids experience an increase in temperature and go into the fluid phase, and alternatively it occurs when the fluid phase is cooled down. The observation of this phase transition process is characterized by a melting point temperature of the ripple phase to fluid phase, nucleation point and growth directionality for the formation of the ripple phase. HS-AFM coupled to a temperature-controlled system can report directly ripple to fluid phase transitions (reversibly) in real time and at high resolution (Takahashi et al., 2016). Transition processes from ripple phase to fluid phase and from ripple phase to metastable ripple phase to fluid phase, could be reversibly, phenomenologically and quantitatively studied. In Takahashi *et al.*, results showed phase transition hysteresis in fast cooling and heating processes, while both melting and condensation occurred at 24.15 °C in quasi-steady state situation. A second metastable ripple phase with larger periodicity was formed at the ripple phase to fluid phase transition when the buffer contained Ca^{2+}. Thermodynamically, a lipid system containing small domains does not necessarily correspond to a phase coexistence regime, but they may constitute a one phase regime with micro- or nanoscale heterogeneities[1] (Heimburg, 2000). Altogether, these findings

[1] We will further visit this topic in Section 5).

may have relevance in more complex cellular systems where lipid nanodomains form and dissociate reversibly.

4.2 Phase coexistence

Phase segregation and coexistence in lipid bilayers generally happens in the simplest models when mixing a fluid and a gel-like phospholipids, and in the more complex mixtures, like those containing phospholipids, sphingomyelins, ceramides, and cholesterol. At room temperature the bilayers composed of a mixture of a gel and a fluid phospholipid generally segregate into different domains, showing a continuous fluid phase enriched with l_d lipid and thicker dispersed domains associated to a phase enriched in the s_o lipid. When the T_m of the gel-phase lipid is overcome, the binary phospholipid system becomes homogeneous and fluid. Among the many that can be found in the literature, we here mention some examples of these binary systems.

The capability of QCM-D to detect lateral phase coexistence and map phase diagrams for binary lipid mixtures of saturated phospholipids will be provided for binary mixtures of homologous phosphatidylcholines DMPC and DSPC, whose chemical structures differ in four methylene groups. This system has been thoroughly investigated experimentally and theoretically in free standing lipid systems (Ehrig et al., 2011; Fidorra et al., 2009; Mabrey & Sturtevant, 1976). DMPC:DSPC mixing behavior is driven by the large hydrophobic mismatch between the two components and departs from ideality as a consequence of the large difference in T_m of the pure constituents.

Figure 9 (left panel) shows representative QCM-D signature of phase transitions we now revisit taking place upon heating pure SVLs of pure DMPC and three DMPC:DSPC mixtures (Losada-Pérez, Mertens, et al., 2015). The diameter of the precursor vesicles forming the SVLs was around 130 nm. For pure DMPC, the main transition takes place in a rather narrow temperature range around $T_m \sim 24$ °C. The first-order derivatives of Δf curves capture the typical behaviour of two-component lipid mixtures displaying s_o and l_d phase coexistence. As very low DSPC concentration (DSPC mole fraction = 0.1), the transition is shifted towards higher temperatures and takes place in a broader temperature range indicating a loss of intermolecular cooperation between DMPC molecules to undergo the main transition due to the presence of DSPC. For the mixtures close to the equimolar concentration two small peaks can be observed indicating the coexistence of two phases, s_o and l_d. The peaks are not simple additions of the peaks of the individual constituents, the size of each peak scales with the concentration of each lipid in each coexisting phase. For instance, the inset of Figure 9 displays the peaks of the mixture DMPC:DSPC (40:60). The low-temperature peak corresponds to the DMPC-rich phase, while the

high-temperature peak to the DSPC-rich phase. As expected, the size of the latter is higher, since the concentration of DSPC in the mixture is larger.

The analysis of the peaks using the tangent method (Ehrig et al., 2011) to determine the onset and completion temperatures enables to map the phase diagram of this mixture. The solid lines are added as a guide to the eye, delimiting the phase coexistence region, dark red (liquidus line), light blue (solidus line) and follow experimental heat capacity values by Maubrey *et al*. (Mabrey & Sturtevant, 1976) obtained for multilamellar vesicles of the same concentration.

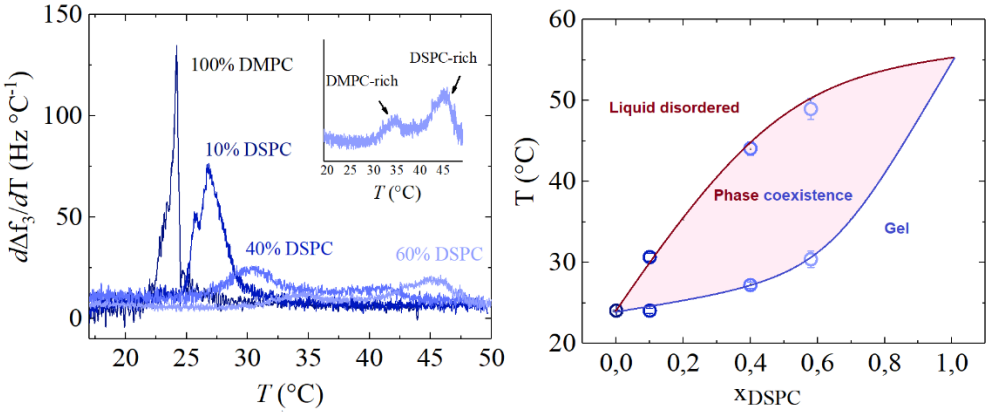

Figure 9. Left panel: temperature profiles of the first-order temperature derivative of the frequency shifts for pure DMPC and DMPC:DPSC mixtures 10%, 40% and 60% mole fraction (in percentage) of DSPC. Right panel: phase diagram obtained from extracting onset and completion temperatures from the peaks (Losada-Pérez, Mertens, et al., 2015).

As discussed in the previous sections, the nanomechanical properties determined by AFM-FS on SLBs are distinctive of the chemical structure and molecular organization of a bilayer at specific environmental conditions. This allows for a direct correlation of the elastic modulus, F_b, or F_{tube} values with the composition in phase-segregated membranes. In most cases, the AFM topographical characterization easily identifies the segregation of an SLB in different domains, due to their difference in thickness and compressibility. However, it is possible to reveal the presence of different domains in an SLB on the basis of their different mechanical properties even when the domains have a height difference which is too small to be detected by conventional imaging.

Bernchou *et al*. studied, using combined fluorescence microscopy and AFM, the nucleation and growth of domains in equimolar binary SLBs composed by DOPC and DPPC (Bernchou et al., 2009), a mixture that shows coexistence of l_d and s_o domains at room temperature (Z. V. Leonenko et al., 2004). These authors could observe that during cooling the shape of the domains evolved from compact to a branched morphology, which they discussed as the domain

growth being controlled by the diffusion of DPPC from the liquid phase toward the solid domain interface. In the late stages of the growth, the size and overall shape of the domains depend on the position of the nucleation points relative to the surrounding nucleation point positions.

A mechanical contribution concerning the elastic deformation of the membrane before the breakthrough point should be considered to fully comprehend the force-distance curve. A method to study the elastic properties consists of quantitative nanomechanical mapping (Picas et al., 2012). In (L Redondo-Morata et al., 2016), the equimolar binary lipid mixture DPPC:DOPC was studied, where l_d and s_o coexisting domains in SLBs are large and directly visually discernable by AFM imaging (Figure 10a) with clearly distinguishable heights (~0.8 nm height difference, Figure 10b). Elastic modulus nano-mechanical mapping (Figure 10c) shows good agreement with the *E* values in the literature, characterized mechanically by AFM (Picas et al., 2012; Rawicz et al., 2000) and micropipette aspiration (Dieluweit et al., 2010). The mean *E* values are 26^{+58}_{-12} MPa for the l_d domain and 33^{+75}_{-15} MPa for the s_o domain, respectively (Figure 10d).

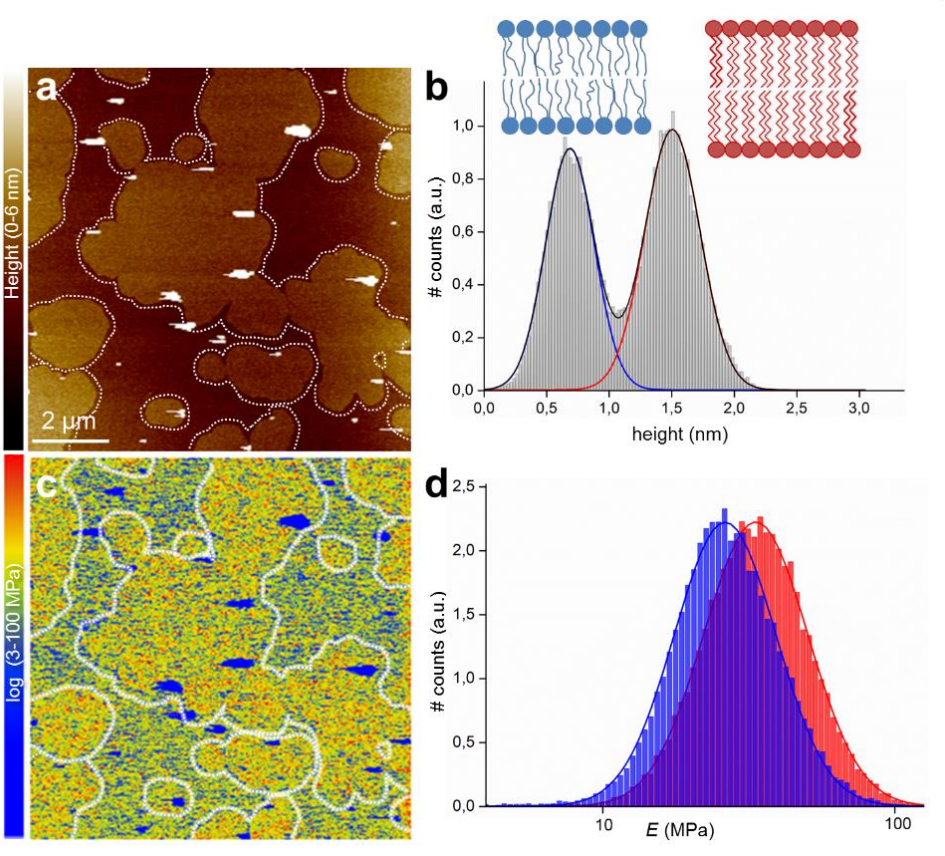

Figure 10. PF-QNM AFM Topography and Elasticity mapping of DOPC:DPPC (1:1) SLBs. a) Topography image (nm) and b) height histogram analysis of the topography (a). The dashed lines in a) represent the domain edges defined by edge detection. The solid lines in b) are Gaussian fits to the height distribution, indicating an average height difference between the DOPC l_d (blue line)

and DPPC s_o (red line) domains of 0.82 nm. c) The corresponding stiffness map (log scale, MPa) and d) Young's modulus values histograms (log scale, MPa) of the regions outlined in the topography (a) and stiffness (c) maps, corresponding to the DOPC (blue) and DPPC (red) domains. The solid lines are Gaussian fits to the distributions peaking at 26^{+58}_{-12} Mpa (DOPC) and 33^{+75}_{-15} Mpa (DPPC) (from reference (L Redondo-Morata et al., 2016) with permission).

Using the Young modulus for each domain of the DOPC:DPPC mixture together with the experimental bilayer thickness (h), the thin shell theory can be used to calculate the area compression-expansion modulus (K_A) and bending modulus (k_C) as (Rawicz et al., 2000):

$$K_A = \frac{Eh}{(1-\nu^2)} \quad \text{and} \quad k_c = \frac{Eh^3}{24\,(1-\nu^2)}$$

When lipid domains separate in lipid mixtures, or when lipids surround membrane embedded proteins there is, in general, a hydrophobic mismatch at the domain interfaces (Wallace et al., 2006) or protein/bilayer interfaces (Mouritsen & Bloom, 1984), with an ensuing compression or stretching of the hydrocarbon chains in the vicinity of the interface. This hydrocarbon tail stretching or compression may influence the distribution of domain sizes and the kinetics of domain separation, as well as membrane protein function. The compression/stretching of the acyl chains of the s_o and l_d domains can be determined by minimizing the elastic energy of the system, $G_s(x)$, expressed assuming volume conservation (Wallace et al., 2006) as

$$G_s = \frac{K_O A_O}{2h_O^2}(x - h_O)^2 + \frac{K_D A_D}{2h_D^2}(x - h_D)^2 \qquad (2)$$

where K_o and K_d are the stretch moduli for s_o and l_d, respectively. A_o and A_d are the lipid area per molecule for s_o and l_d, respectively. A values are well-documented in literature (notably through X-ray diffraction and Langmuir methods), being 0.72 nm^2 for l_d DOPC and 0.49 nm^2 for s_o DPPC at room temperature (Nagle & Tristram-Nagle, 2000). h_o and h_d are the measured bilayer thickness of s_o and l_d, respectively. The estimated G_s values for the DOPC l_d and the DPPC s_o domains are 0.27 k_BT. Hence, the experimental determination of E allows to estimate the stretch modulus and the bending stiffness of the lipid membrane, as well as the energetic cost of the lipid domains to accommodate to different thickness.

For the SLB system composed of a POPE:POPG mixture (Picas et al., 2009), AFM images revealed the existence of two separated phases, the higher showing a region with protruding subdomains. AFM-FS was then used to clarify the nature of each phase. The values of F_b, adhesion force and height extracted from the force curves were assigned to the corresponding s_o (the mechanically stable domains) and l_d phase (the mechanically labile phase). In Crespo-

Villanueva *et al.*, while the SLB composed of equimolar DSPC:DOPC was shown to phase segregate, clearly demonstrated in the AFM topographical images and the correlative F_b maps and bimodal distributions around ~40 nN and ~5 nN, the equimolar mixture of the two l_d lipids DOPC:DOPS led to a homogeneous topography and narrow F_b distribution around 3.5 nN (Crespo-Villanueva et al., 2018). In Domenech *et al.*, they studied ternary mixtures of POPC:POPE:CL, a minimum system that mimics the mitochondrial inner membrane (Domenech et al., 2007). They could observe laterally segregated domains whose height decreased with increasing temperatures.

Pulling lipid tubes with the AFM probe also allows to characterize phase segregated bilayers and laterally resolve the different domains in multicomponent SLBs (Berta Gumí-Audenis et al., 2018). This is exemplified in Figure 11, a bilayer composed of the l_d lipid DOPE and the s_o lipid DPPG in ratio DOPE:DPPG 25:75, that at room temperature forms SLB patches with coexisting domains: gel-phase rich in DPPG, dispersed in fluid-phase rich in DOPE. When indented by the AFM tip at a constant velocity of 1 µm s^{-1}, a bimodal F_b distribution is obtained, with differentiated mean F_b values associated with the fluid (~5 nN) and gel (~12 nN) domains. Analyzing the retract force-separation curves that showed the tube pulling event allowed to represent the F_{tube} distribution and map, where the lower force values (red pixels) are distributed in the peripheral part of the SLB patch and higher forces (yellow pixels) in the center, and the F_{tube} distribution is resolved when sorting according to the corresponding F_b, giving a mean value of 75 ± 20 pN for the DOPE-rich phase, and 112 ± 25 pN for the DPPG-rich phase. The fact that F_b and F_{tube} for the domains slightly differ from the values for pure DOPE and DPPG SLBs allows to infer partial miscibility among them.

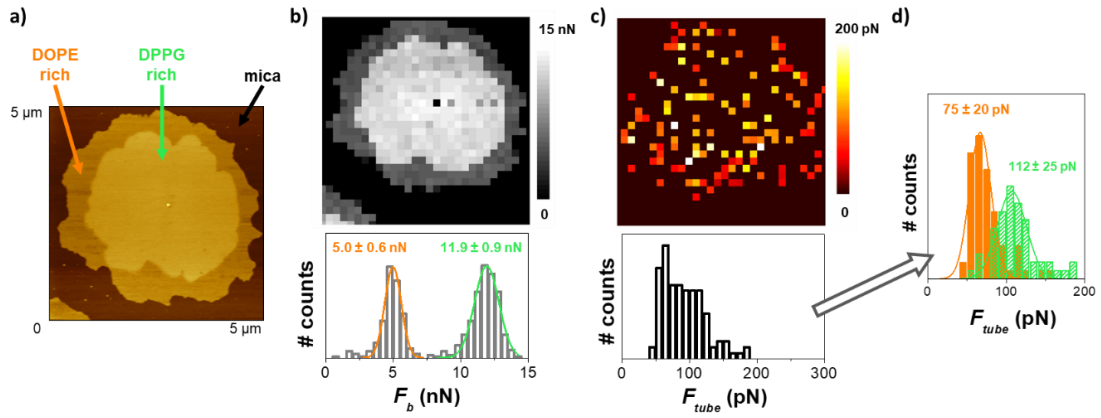

Figure 11. DOPE:DPPG (25:75). a) AC-mode AFM topographical image; b) F_b map and distribution; c) F_{tube} map and distribution; d) F_{tube} distributions resolved by filtering according to the F_b

distribution. Reproduced from Ref. (Berta Gumí-Audenis et al., 2018) with permission from the Royal Society of Chemistry.

Higher complexity models, like the ternary lipid mixtures containing an unsaturated phosphatidylcholine (PC), a saturated PC or sphingomyelin (SM), and Cholesterol (Chol) have been probably the most studied due to the physiological abundance of these lipids. Depending on the ratio of the components, these mixtures have shown to exhibit two coexisting fluid phases: an l_o phase that is enriched in Chol and SM or saturated PC, and an l_d phase that is predominantly composed of unsaturated PC (Johnston, 2007), and the possibility of a coexisting s_o phase. The group of Schwille has extensively analyzed the domain organization in DOPC/SM/Chol model membranes by means of AFM in combination with fluorescence correlation spectroscopy (FSC) (S Chiantia, Kahya, et al., 2006; S Chiantia, Ries, et al., 2006; Salvatore Chiantia et al., 2007, 2008) and by performing AFM-FS experiments on the different phases they have shown that the average force needed to pierce the l_o phase of the DOPC/SM/Chol bilayer is about 4 nN higher than the one needed to pierce the l_d phase. In a parallel study, Zou and coworkers explored the influence of different cholesterol contents on the morphology and (nano)mechanical stability of phase-segregated DOPC/SM/Chol lipid bilayers by means of AFM imaging and force mapping (R M A Sullan et al., 2010). They observed consistently higher F_b values in the SM/Chol-enriched l_o domains than in the DOPC-enriched l_d phase, and that the (nano)mechanical stability of both coexisting phases counterintuitively decreased with increasing Chol content. By following the dependence of the F_b value with the loading rate in both phases, they calculated the activation energies (ΔE_0) of bilayer rupture at zero applied force. ΔE_0 values obtained were in the range 75-125 kJ/mol for all tested Chol contents and did not show a dependence on the different lipid phases.

Besides sphingolipids, ceramides (Cer) have also gained attention in physicochemical studies by means of AFM, since they are known to be predominant in physiologically relevant nanodomains -which have been controversially called for many years lipid rafts (Goñi, 2019a). Longo and coworkers observed that DLPC/GalCer/Chol ternary mixtures only display l_d/s_o coexistence and no l_o phase even at high Chol content (Blanchette et al., 2006). By measuring the area/perimeter ratios of the segregated domains, the authors concluded that Chol was able to decrease the line tension between the two phases. In another study (W.-C. Lin et al., 2007), they could also observe a phase coexistence attributed to l_d/l_o phases with POPC and DOPC at 10 mol% Chol, an indication that fatty acyl chain unsaturation, cholesterol ratio and lipid hydrophobic mismatch in the organization of multi-component lipid systems.

Ceramide incorporation on coexisting fluid phase and ordered domains in phase-separated binary and ternary lipid mixtures was shown to affect the lipid spatial organization in domains, with the appearance of a Cer-enriched gel-like phase and the displacement of cholesterol from rafts (S Chiantia, Kahya, et al., 2006; Salvatore Chiantia et al., 2007; Ira et al., 2009). In order to directly probe and quantify the (nano)mechanical stability and rigidity of the Cer-enriched platforms, Zou *et al*. performed AFM topographical images and force mapping that allowed the determination of the F_b value and elastic modulus of the different phases (Ruby May A Sullan et al., 2009a, 2009b; Zou & Johnston, 2010). They confirmed the expulsion of cholesterol from sphingolipid/Chol-enriched domains as a result of Cer incorporation, and observed an increased mechanical stability attributed to the influence of Cer in the lipid organization and packing behavior, also reported later on GalCer rich domains on model membranes with PC and Chol (Berta Gumí-Audenis et al., 2015).

The group of Goñi has systematically explored the effect of the acyl compositions of sphingomyelins and the corresponding ceramide counterparts in ternary mixtures with PC and Chol (García-Arribas et al., 2016; González-Ramírez et al., 2019; Jiménez-Rojo et al., 2014)). Combining confocal microscopy, DSC, AFM imaging and FS, they compared the effects of C24:1 Cer (nervonoyl ceramide, nCer) with those of C16:0 Cer (palmitoyl ceramide, pCer) in bilayers composed basically of DOPC, SM (either C24:1, nSM or C16:0, pSM) and Chol (García-Arribas et al., 2017). AFM-FS showed that nCer has a lower stiffening effect than pCer, while the presence of nSM reduces the stiffness. When the proportion of phospholipid increases beyond 60 mol %, a lateral phase separation occurs at the micrometer scale (González-Ramírez et al., 2019). The authors interpreted this data as a pCer:Chol interaction, that would predominate at the lower phospholipid concentrations. The putative pCer:Chol complexes (or nanodomains) would mix well with the phospholipid. At higher SM concentrations pSM:pCer and pSM:Chol interactions would become more important, giving rise to the coexisting s_o and l_o phases, respectively. Heterogeneity, or lateral phase separation, occurs more easily with pSM than with DPPC, indicating a higher affinity of SM over DPPC for Chol or Cer. Altogether, the findings of Goñi and coworkers show the sharp increase in complexity when membranes exhibit different sphingolipids of varying N-acyl chains, which should be a common issue in an actual cell membrane environment.

1.2. The role of cholesterol

Cholesterol is a fundamental constituent of the eukaryotic cell plasma membranes. Eukaryotic cell membranes are not entirely in the conventional l_d phase. Instead, they are, at least partially, in the Chol-rich liquid-ordered (l_o) phase or a phase with similar properties. l_o phase is

characterized by a high degree of acyl chain order and is favored by high-T_m lipids with saturated acyl chains such as sphingolipids, when they are mixed with Chol, as exposed in the previous section. Chol plays the essential function of regulating the physical properties of the cell membrane as it controls the lipid organization and phase behavior, regulates the membrane fluidity and its mechanical strength, influencing the passive permeability of water and other small molecules (Pan et al., 2008; Pinkwart et al., 2019). From the molecular perspective, Chol is considered to produce a condensing effect and induce ordering to fluid phase lipids forming the membrane and to have the opposite effect on phospholipids present in the gel phase (Hung et al., 2007; Rog et al., 2009). However, several experiments pointed out the complex effect of Chol on lipid bilayers, which depends on the molecular structure of the neighboring lipids: the degree of chain unsaturation, the length of the hydrophobic tail and the chemistry of the headgroup (Pan et al., 2008; Mills et al., 2009; Garcia-Manyes et al., 2010). In view of acknowledging the particular role of cholesterol, let us briefly outline results on the phase behavior of SVLs and SLBs consisting of binary mixtures of saturated phospholipids and cholesterol using mechanical descriptors such as shear viscosity of SVLs and nanomechanics of SLBs.

We first describe the phase behavior of SVLs containing binary mixtures of DMPC:Chol using QCM-D. Upon the addition of Chol to phospholipid bilayers, the sharp main phase transition in pure DMPC gradually diminishes and eventually disappears over a given Chol concentration. In the case of DMPC, SVLs showed no transition from 30% cholesterol. Figure 12 shows normalized shear viscosity η_{norm} =[$\eta(t)/\eta(t=0)$, with t the time] for pure DMPC and DMPC:Chol (20 mol % Chol) calculated using a Voigt-based viscoelastic model (Voinova et al., 1999). At intermediate Chol concentrations, asymmetric peaks can be observed. These peaks encompass two main contributions, a sharp, narrow peak and a broader one that overlaps with the former (see right panel in Figure 12 for a more detailed view including Gaussian fitting). Two domains can be identified, namely, the sharp contribution can be ascribed to the pure DMPC-rich domains undergoing the main transition and the latter to the Chol-rich ones. The broader peak appears as a result of the reduced mobility of the hydrophobic chains of DMPC in Chol-rich domains. The presence and the size of these domains depend strongly on the concentration of cholesterol and the temperature. On increasing the amount of cholesterol, the temperature range of the overall transition increases as a result of the extension of the second broad contribution, while the size of the maximum corresponding to the melting of the single lipid decreases. No phase transition is detected at Chol concentration over 30 mol % indicating the formation of a homogeneous liquid ordered l_o phase at a macroscopic level. Such a large cholesterol concentration inhibits

the formation of extended domains. A similar pattern of behavior was observed for DPPC:Chol SVLs, however, for this later system, the completion temperature of the overall transition at intermediate cholesterol concentrations was not attained, due to the (upper) limited temperature range of commercial QCM-D systems (Losada-Pérez, Khorshid, et al., 2015). These results are in agreement with recent calorimetric studies of free-standing membranes of the same systems (Mannock et al., 2010).

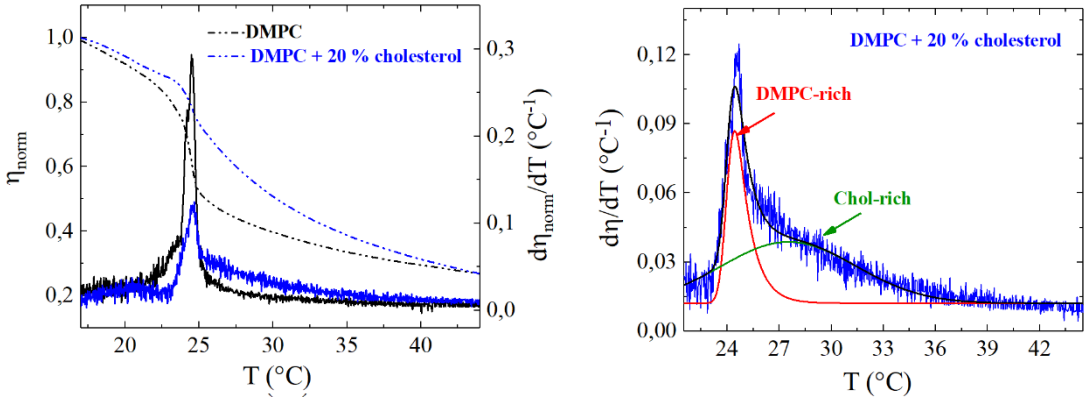

Figure 12. Left panel Temperature dependence of the normalized effective shear viscosity (dash dotted lines) and its first-order derivative (solid line) of DMPC and DMPC + 20% cholesterol SVLs on a supported vesicle layer on a gold-coated QCM-D quartz sensor upon heating. Right panel closer view of the normalized shear viscosity first-order derivative for DMPC + 20% cholesterol SVLs. Solid lines denote multiple peak gaussian fitting.

The role of Chol in the structure and nanomechanics of SLBs has been extensively studied by AFM (L Redondo-Morata et al., 2012b; R M A Sullan et al., 2010; Al-Rekabi & Contera, 2018; S Garcia-Manyes et al., 2010; Adhyapak et al., 2018), as well as its interplay with sphingolipids or other lipids (García-Arribas et al., 2016; 2006; Ahyayauch et al., 2002; Guyomarc'h et al., 2014) and further reviewed in (B. Gumí-Audenis et al., 2016b).

By means of temperature-controlled AFM imaging and AFM-FS to assess the influence of Chol on the membrane ordering and stability (Redondo-Morata et al., 2012), this work analyzed a DPPC:Chol in representative range of compositions up to 50 mol % Chol, studying the phase evolution upon heating (from room temperature to temperatures high above the T_m of DPPC) and the corresponding (nano)mechanical stability. This provided a correlation between the mechanical behavior and composition with the lateral order of each phase present in the bilayers. It proved that low Chol contents lead to a phase segregated system, while high contents of Chol can give a homogeneous topography, although a bimodal F_b distribution was observed, possibly due to the presence of small heterogeneities that could not be resolved in the images. In all cases, it was demonstrated that Chol enhances the mechanical stability of the binary

membrane, and an extraordinarily stable system was observed for equimolar fractions (50 mol % Chol). In addition, even when no thermal transition was detected by the traditional bulk analysis techniques for vesicles with high Chol content (40 and 50 mol %), it was shown that temperature-controlled AFM-FS is capable of identifying a thermal transition for the SLBs. As detailed in Figure 13, for high-Chol contents -40 and 50 mol %- the DPPC:Chol system shows a double F_b distribution at room temperature, probably due to the presence of (space or time) non-resolved heterogeneities for these compositions. Although no thermal transition was observed in DSC thermograms of free-standing systems, when AFM-FS experiments were performed at different temperatures for these systems, a gradual decrease of the mean F_b value was observed until temperature reached ca. 40 °C. The continuous decrease in the F_b value with increasing temperature may be ascribed to an increase in fluidity of the system, and it is evident that, although not detected in DSC of DPPC:Chol vesicles, a transition occurs for DPPC:Chol SLBs with 40 and 50 mol % Chol around 42-45 °C. Below this temperature, the system in the l_o phase presents extraordinary lateral order and may have properties that resemble a gel-like bilayer, and as temperature increases, it gradually becomes a system with higher lateral mobility (but still with higher order than the DPPC l_d phase). This behavior indicates that for DPPC:Chol SLBs, a thermal transition occurs even for high-Chol compositions, in a temperature range between ca. 42-47 °C independently of the membrane composition, and that it may probably be of second-order for the high-Chol DPPC:Chol bilayers (40-50 mol %), which generally appear as a very broad transition or it is even not detected in DSC experiments of free standing vesicles or QCM-D of SVLs.

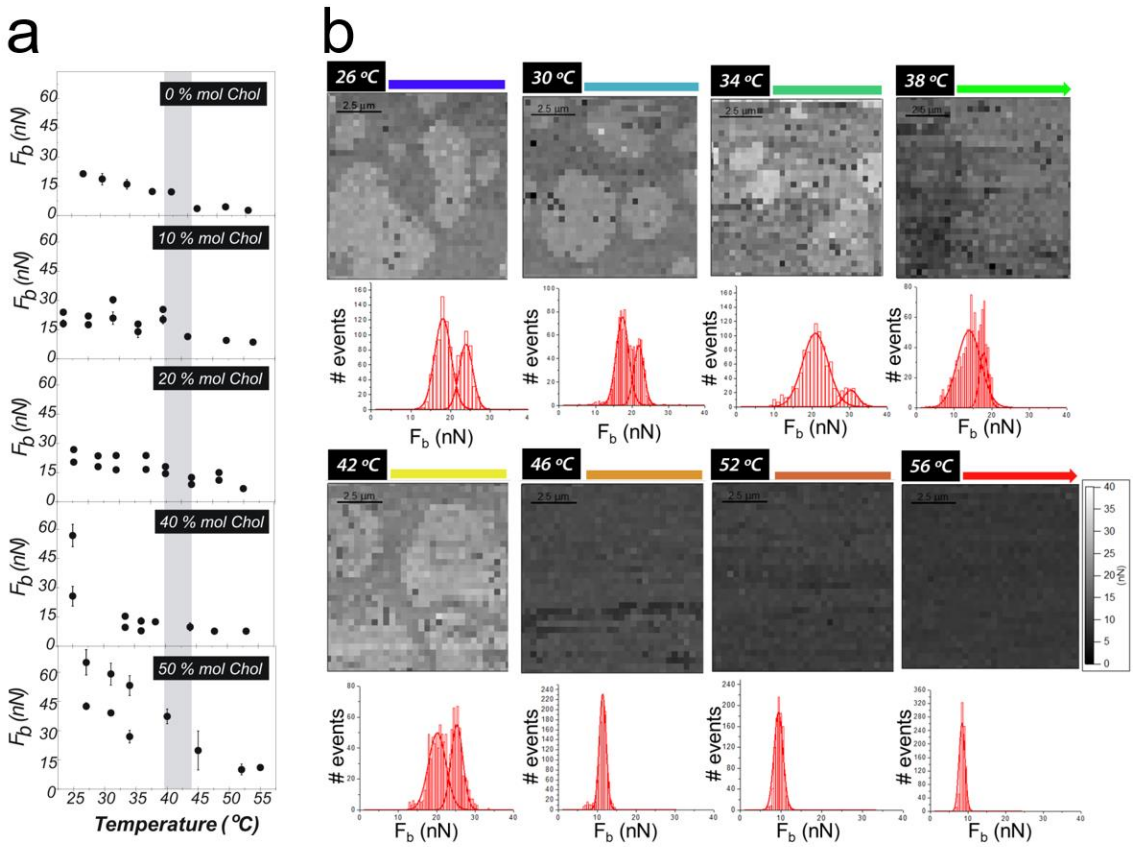

Figure 13. a) Mean F_b value of DPPC:Chol SLBs in 10 mM HEPES, 20 mM $MgCl_2$ and 150 mM NaCl, pH 7.4, with various Chol contents, as a function of temperature. The shadowed vertical line marks the temperature range where the main transition in pure DPPC occurs. For DPPC:Chol SLBs with 40 and 50 mol % Chol, although not detected in DSC of DPPC:Chol vesicles, a transition occurs around 42–45 °C. b) F_b maps and distributions for DPPC:Chol SPB with 10 mol % Chol, in 10 mM HEPES, 20 mM $MgCl_2$ and 150 mM NaCl, pH 7.4, with increasing temperature. Reprinted from (L Redondo-Morata et al., 2012b).

Strikingly, information about the lateral in-plane structure of such systems can be instead obtained by grazing incidence XR diffraction (GIXD). In (Gumi-Audenis et al., 2018), a silicon-SLB system was designed in order to deal with the requirement of the wetting preservation to guarantee the membrane stability while minimizing the background from the liquid environment. Using this methodology, it was confirmed that DPPC:Chol with low contents of Chol up to 30 mol % lead to separation into two coexisting phases at room temperature and concentrations higher than 30 mol % Chol appear to be a unique l_o phase. This condition was consistent with the earlier work (Redondo-Morata et al., 2012b) demonstrating that such increase of nanomechanical resistance is associated to a strong lateral interaction mediated by Chol molecules placed between the DPPC ones, due to a highly stable structure with most probably an equimolar DPPC:Chol ratio.

To date, efforts continue to understand the complex role of cholesterol in biomembranes. Still, these discoveries cannot always be directly translated to the behavior of living cell membranes. By means of advanced fluorescence imaging and spectroscopy, Sezgin and colleagues (Pinkwart et al., 2019) have shown that cholesterol diffuses faster than phospholipids in live membranes, but not in model membranes. Interestingly, a detailed statistical diffusion analysis suggested two-component diffusion for cholesterol in the plasma membrane of live cells.

Recent work based on a systematic AFM-FS study on DOPC:Chol SLBs at varying ratios suggested, however, that cholesterol may not just be responsible of increasing the mechanical stability but also introduce irregularities across the leaflets (Adhyapak et al., 2018). At Chol ratios above 20%, they could observe two sudden jumps in the force-distance curve, the second jump always displaying shorten separation. They interpreted that cholesterol induced asymmetry across the (in the inner and outer leaflets) bilayer, related to the phenomena of interleaflet coupling and depending on Chol concentration.

Recently, Contera and coworkers took a different approach to study the effect of Chol in the mechanical properties of lipid bilayers (Al-Rekabi & Contera, 2018). Applying different frequencies simultaneously in an AFM topography mode, namely amplitude modulation–frequency modulation (AM–FM), they investigated the effect of Chol on DPPC bilayers in concentrations from 0 to 60 %. The lipid bilayers probed with this methodology displayed both elastic and viscous behavior. Cholesterol showed to modulates both, increasing elastic and viscous components as a function of Chol concentrations. The authors interpreted that their results may have a physiological relevance, where such viscoelastic properties may be used by cells to modulate the propagation (elastic) or attenuation (viscous) of mechanical signals across the cell membrane.

5. Connection between nanoscale measurements and thermodynamic descriptors of membranes

When studying phase coexistence in lipid membranes a distinction between thermodynamically stable phases and transient local domains in lipid bilayer at equilibrium should be made. Let us briefly discuss this in line with the above-exposed results on phospholipid-cholesterol binary mixtures. PC-Chol binary mixtures have been studied for many years using a plethora of experimental techniques. Yet, despite their apparent simplicity being two-component systems, their phase behavior remains controversial and, in many cases, departs from the canonical phase diagram proposed by Vist and Davis (Vist & Davis, 1990). In fact, results depend strongly on the

spatio-temporal resolution of the different experimental techniques. For instance, unlike predicted by most phase diagrams, l_d-l_o phase coexistence was not observed for micron-sized GUVs of DPPC-cholesterol mixtures using fluorescence microscopy (Veatch & Keller, 2003), while some other techniques captured this phenomenon for free standing MLVs vesicles (DSC (Mannock et al., 2010), volumetric (Miyoshi et al., 2014), NMR (Davis et al., 2009), SLBs (AFM)(L Redondo-Morata et al., 2012b), and SVLs (QCM-D)(Losada-Pérez, Khorshid, et al., 2015). These findings suggest that, instead of macroscopic phase separation, these systems are presumably filled with mesoscopic and nanoscopic domains, whose size and lifetime depends on temperature and mixture composition (Winkler et al., 2017).

Classically, when dealing with phase separation the Gibbs' phase rule is customarily invoked, assuming macroscopic phase coexistence and neglecting the role of phase boundaries, which comparably, hardly contribute to the free energy. If domains are small, the interfaces between domains constitute an important part of the system and its contribution to the free energy is not negligible. In this respect, using the term phase in the classical thermodynamic sense might not be appropriate (Heimburg, 1998; Almeida et al., 2005). Following Hill (Hill, 2013) a system can no longer be called a phase when it ceases to behave like a macroscopic system and starts behaving like a small system.

In this respect, both AFM and QCM-D have demonstrated to be valuable tools to detect domain (nano/mesoscopic sized domains) coexistence within supported membranes of binary lipid mixtures.

6. Conclusions and future perspectives

As mentioned in the previous sections, AFM-FS can interestingly resolve coexistence of domains at concentrations where height differences at domain boundaries are not detectable. Breakthrough force thus stands as a useful mechanical descriptor to resolve domain coexistence. Even though domains cannot be considered as phases in the purely thermodynamic standpoint, this does not mean that these systems cannot be treated in a rigorous thermodynamic way. As a matter of fact, the breakthrough force is able to detect a thermal transition at high cholesterol concentrations in binary PC:Chol SLBs, whose origin deserves to be revisited and further explored in the framework of either fluctuations arising in the vicinity of a critical point, the possibility of glassy-cholesterol-rich nanodomains or eventual cholesterol crystallization. In this sense, the development of HS-AFM will likely provide new insights due to its unprecedented spatio-temporal resolution, thanks to a direct correlation between structure and diffusion (Munguira et al., 2016). Similarly, HS Force Spectroscopy has the capacity to cover a wider force

spectrum, which can help to validate theoretical frameworks of the field, as well as provide a direct correlation with Molecular Dynamics simulations (Rico et al., 2013).

There is indeed plenty of room in fundamental lipid biophysics and phase behavior in particular to use both purely mechanical and viscoelastic properties as descriptors to provide a more complete picture of the origins of domain formation and coexistence. The ultimate lipid phase coexistence to be fully understood are transient nanodomains, often (confusively) referred to as lipid rafts. There is to date no agreement about the size and lifetime of rafts, and the term is used to referred to a collection of different structures (Goñi, 2019). Based on the current knowledge, microdomains in equilibrium are no longer considered suitable models for the biological structure that rafts represent. Fortunately, advanced super-resolution microscopies and fast techniques are becoming available and will shed some light in one of the most discussed topics in biomembrane studies.

In light of this, multiscale spatio-temporal measurements of mechanical properties of supported membranes can help to experimentally address different scenarios where membrane micro- and nano-domain formation finds theoretical support. Starting from equilibrium ternary lipid mixtures in the vicinity of a critical point, it might be worth exploring how the presence of critical fluctuations reflects in the membrane mechanical properties, and if these properties can be used as physical descriptors to test critical-point universality laws. Secondly, tuning membrane (local and global) environment by actively controlling curvature, leaflet asymmetry, solid support topography and addition of external components would help complete the manifold where domain formation occurs. Finally, the growing spatiotemporal capabilities of AFM are promising tools to explore membrane organization in the realm of non-equilibrium phenomena.

7. Acknowledgements

We acknowledge financial support from the Generalitat de Catalunya (2017-SGR-1442), the Instituto de Salud Carlos III, through “Acciones CIBER” and CIBER-BBN FlexQS-skin and FelxCAB projects. This work was also supported by a grant overseen by the French National Research Agency (ANR) as part of the “Investments d’Avenir” Programme (I-SITE ULNE / ANR-16-IDEX-0004 ULNE) to L.R.-M. Financial support from the project ‘SADI’ by the programme Action Recherche Concertée, Université Libre de Bruxelles (ULB) to P.L-P is also acknowledged.

8. Glossary of lipid acronyms

Acronym	Long name

C16:0 palmitoyl Cer (aka palmitoyl Cer, pCer)	N-palmitoyl-D-erythro-sphingosine
C16:0 palmitoyl SM (aka palmitoyl SM)	N-palmitoyl-D-erythro-sphingosylphosphorylcholine
C24:1 nervonoyl Cer (aka nervonoyl Cer, nCer)	N-nervonoyl-D-erythro-sphingosine
C24:1 nervonoyl SM (aka nervonoyl SM)	N-Nervonoyl-D-erythro-sphingosylphosphorylcholine-d9
Cer	ceramide
Chol	cholesterol
CL	cardiolipin
DMPC	1,2-dimyristoyl-sn-glycero-3-phosphocholine
DOPC	1,2-dioleoyl-sn-glycero-3-phosphocholine
DOPE	1,2-dioleoyl-sn-glycero-3-phosphoethanolamine
DOPG	1,2-dioleoyl-sn-glycero-3-[phospho-rac-(3-lysyl(1-glycerol))]
DOTAP	1,2-dioleoyl-3-trimethylammonium-propane
DPPA	1,2-dipalmitoyl-sn-glycero-3-phosphate
DPPC	1,2-dipalmitoyl-sn-glycero-3-phosphocholine
DPPE	1,2-dipalmitoyl-sn-glycero-3-phosphoethanolamine
DPPG	1,2-dipalmitoyl-sn-glycero-3-phospho-(1'-rac-glycerol)
DSPC	1,2-distearoyl-sn-glycero-3-phosphocholine
GalCer	Galactosylceramides
PC	phosphocholine
PE	phosphoethanolamine
POPC	1-palmitoyl-2-oleoyl-glycero-3-phosphocholine
POPE	1-palmitoyl-2-oleoyl-sn-glycero-3-phosphoethanolamine
POPG	1-palmitoyl-2-oleoyl-sn-glycero-3-phospho-(1'-rac-glycerol)
SM	sphongomyelin

9. References

Adhyapak, P. R., Panchal, S. V., & Murthy, A. V. R. (2018). Cholesterol induced asymmetry in DOPC bilayers probed by AFM force spectroscopy. *Biochimica et Biophysica Acta (BBA) - Biomembranes*, *1860*(5), 953–959. https://doi.org/10.1016/j.bbamem.2018.01.021

Ahyayauch, H., Requero, M. A., Alonso, A., Bennouna, M., & Goni, F. M. (2002). Surfactant effects of chlorpromazine and imipramine on lipid bilayers containing sphingomyelin and cholesterol. *Journal of Colloid and Interface Science*, *256*(2), 284–289. https://doi.org/10.1006/jcis.2002.8690

1149 Alessandrini, A., & Facci, P. (2012). Nanoscale mechanical properties of lipid bilayers and their
1150 relevance in biomembrane organization and function. *Micron*, *43*(12), 1212–1223.
1151 https://doi.org/10.1016/j.micron.2012.03.013
1152 Almeida, P. F. F., Pokorny, A., & Hinderliter, A. (2005). Thermodynamics of membrane
1153 domains. *Biochimica et Biophysica Acta (BBA) - Biomembranes*, *1720*(1), 1–13.
1154 https://doi.org/10.1016/j.bbamem.2005.12.004
1155 Al-Rekabi, Z., & Contera, S. (2018). Multifrequency AFM reveals lipid membrane mechanical
1156 properties and the effect of cholesterol in modulating viscoelasticity. *Proceedings of*
1157 *the National Academy of Sciences*, *115*(11), 2658–2663.
1158 https://doi.org/10.1073/pnas.1719065115
1159 Ando, T, Uchihashi, T., Kodera, N., Yamamoto, D., Miyagi, A., Taniguchi, M., & Yamashita, H.
1160 (2008). High-speed AFM and nano-visualization of biomolecular processes. *Pflugers*
1161 *Archiv-European Journal of Physiology*, *456*(1), 211–225.
1162 https://doi.org/10.1007/s00424-007-0406-0
1163 Ando, Toshio. (2017). High-speed atomic force microscopy and its future prospects. *Biophysical*
1164 *Reviews*, *10*(2), 285–292. https://doi.org/10.1007/s12551-017-0356-5
1165 Armond, J. W., Macpherson, J. V, & Turner, M. S. (2011). Pulling Nanotubes from Supported
1166 Bilayers. *Langmuir*, *27*(13), 8269–8274.
1167 Bangham, A. D., & Horne, R. W. (1964). Negative staining of phospholipids and their structural
1168 modification by surface-active agents as observed in the electron microscope. *Journal*
1169 *of Molecular Biology*, *8*(5), 660-IN10. https://doi.org/10.1016/S0022-2836(64)80115-7
1170 BANGHAM, A. D., PETHICA, B. A., & SEAMAN, G. V. (1958). The charged groups at the interface
1171 of some blood cells. *The Biochemical Journal*, *69*(1), 12–19.
1172 https://doi.org/10.1042/bj0690012

1173 Barrett, R. C. (1991). High-speed, large-scale imaging with the atomic force microscope.
1174 *Journal of Vacuum Science & Technology B: Microelectronics and Nanometer*
1175 *Structures*, *9*(2), 302. https://doi.org/10.1116/1.585610
1176 Berg, J. M., Tymoczko, J. L., Stryer, L., Berg, J. M., Tymoczko, J. L., & Stryer, L. (2002).
1177 *Biochemistry* (5th ed.). W H Freeman.
1178 Bernchou, U., Ipsen, J. H., & Simonsen, A. C. (2009). Growth of solid domains in model
1179 membranes: Quantitative image analysis reveals a strong correlation between domain
1180 shape and spatial position. *The Journal of Physical Chemistry. B*, *113*(20), 7170–7177.
1181 https://doi.org/10.1021/jp809989t
1182 Binnig, G., Quate, C. F., & Gerber, C. (1986). ATOMIC FORCE MICROSCOPE. *Physical Review*
1183 *Letters*, *56*(9), 930–933. https://doi.org/10.1103/PhysRevLett.56.930
1184 Blanchette, C. D., Lin, W.-C., Ratto, T. V., & Longo, M. L. (2006). Galactosylceramide Domain
1185 Microstructure: Impact of Cholesterol and Nucleation/Growth Conditions. *Biophysical*
1186 *Journal*, *90*(12), 4466–4478. https://doi.org/10.1529/biophysj.105.072744
1187 Brochard-Wyart, F., Borghi, N., Cuvelier, D., & Nassoy, P. (2006). Hydrodynamic narrowing of
1188 tubes extruded from cells. *Proceedings of the National Academy of Sciences*, *103*(20),
1189 7660.
1190 Butt, H. J., & Franz, V. (2002). Rupture of molecular thin films observed in atomic force
1191 microscopy. I. Theory. *Physical Review E*, *66*(3).
1192 https://doi.org/10.1103/PhysRevE.66.031601
1193 Canham, P. B. (1970). The minimum energy of bending as a possible explanation of the
1194 biconcave shape of the human red blood cell. *Journal of Theoretical Biology*, *26*(1), 61–
1195 81.
1196 Chiantia, S, Kahya, N., Ries, J., & Schwille, P. (2006). Effects of ceramide on liquid-ordered
1197 domains investigated by simultaneous AFM and FCS. *Biophysical Journal*, *90*(12),
1198 4500–4508. https://doi.org/10.1529/biophysj.106.081026

1199 Chiantia, S, Ries, J., Kahya, N., & Schwille, P. (2006). Combined AFM and two-focus SFCS study
1200 of raft-exhibiting model membranes. *Chemphyschem*, *7*(11), 2409–2418.
1201 https://doi.org/10.1002/cphc.200600464
1202 Chiantia, Salvatore, Kahya, N., & Schwille, P. (2007). Raft domain reorganization driven by
1203 short- and long-chain ceramide: A combined AFM and FCS study. *Langmuir*, *23*(14),
1204 7659–7665. https://doi.org/10.1021/la7010919
1205 Chiantia, Salvatore, Ries, J., Chwastek, G., Carrer, D., Li, Z., Bittman, R., & Schwille, P. (2008).
1206 Role of ceramide in membrane protein organization investigated by combined AFM
1207 and FCS. *Biochimica Et Biophysica Acta-Biomembranes*, *1778*(5), 1356–1364.
1208 https://doi.org/10.1016/j.bbamem.2008.02.008
1209 Chiaruttini, N., Redondo-Morata, L., Colom, A., Humbert, F., Lenz, M., Scheuring, S., & Roux, A.
1210 (2015). Relaxation of Loaded ESCRT-III Spiral Springs Drives Membrane Deformation.
1211 *Cell*, *163*(4), 866–879. https://doi.org/10.1016/j.cell.2015.10.017
1212 Cho, N.-J., Frank, C. W., Kasemo, B., & Höök, F. (2010). Quartz crystal microbalance with
1213 dissipation monitoring of supported lipid bilayers on various substrates. *Nature*
1214 *Protocols*, *5*(6), 1096–1106. https://doi.org/10.1038/nprot.2010.65
1215 Cho, N.-J., Kanazawa, K. K., Glenn, J. S., & Frank, C. W. (2007). Employing Two Different Quartz
1216 Crystal Microbalance Models To Study Changes in Viscoelastic Behavior upon
1217 Transformation of Lipid Vesicles to a Bilayer on a Gold Surface. *Analytical Chemistry*,
1218 *79*(18), 7027–7035. https://doi.org/10.1021/ac0709504
1219 Choi, S.-E., Greben, K., Wördenweber, R., & Offenhäusser, A. (2016). Positively charged
1220 supported lipid bilayer formation on gold surfaces for neuronal cell culture.
1221 *Biointerphases*, *11*(2), 21003. https://doi.org/10.1116/1.4945306
1222 Clausen-Schaumann, H., Rief, M., Tolksdorf, C., & Gaub, H. E. (2000). Mechanical stability of
1223 single DNA molecules. *Biophysical Journal*, *78*(4), 1997–2007.

1224 Crespo-Villanueva, A., Gumí-Audenis, B., Sanz, F., Artzner, F., Mériadec, C., Rousseau, F., Lopez,
1225 C., Giannotti, M. I., & Guyomarc'h, F. (2018). Casein interaction with lipid membranes:
1226 Are the phase state or charge density of the phospholipids affecting protein
1227 adsorption? *Biochimica Et Biophysica Acta. Biomembranes*, *1860*(12), 2588–2598.
1228 https://doi.org/10.1016/j.bbamem.2018.09.016
1229 Dai, J., & Sheetz, M. P. (1999). Membrane Tether Formation from Blebbing Cells. *Biophysical*
1230 *Journal*, *77*(6), 3363–3370.
1231 Daillant, J., Bellet-Amalric, E., Braslau, A., Charitat, T., Fragneto, G., Graner, F., Mora, S.,
1232 Rieutord, F., & Stidder, B. (2005). Structure and fluctuations of a single floating lipid
1233 bilayer. *Proceedings of the National Academy of Sciences of the United States of*
1234 *America*, *102*(33), 11639.
1235 Davis, J. H., Clair, J. J., & Juhasz, J. (2009). Phase Equilibria in DOPC/DPPC-d62/Cholesterol
1236 Mixtures. *Biophysical Journal*, *96*(2), 521–539.
1237 https://doi.org/10.1016/j.bpj.2008.09.042
1238 Deamer, D. W. (2010). From "banghasomes" to liposomes: A memoir of Alec Bangham, 1921-
1239 2010. *The FASEB Journal : Official Publication of the Federation of American Societies*
1240 *for Experimental Biology*, *24*(5), 1308–1310. https://doi.org/10.1096/fj.10-0503
1241 Dieluweit, S., Csiszar, A., Rubner, W., Fleischhauer, J., Houben, S., & Merkel, R. (2010).
1242 Mechanical Properties of Bare and Protein-Coated Giant Unilamellar Phospholipid
1243 Vesicles. A Comparative Study of Micropipet Aspiration and Atomic Force Microscopy.
1244 *Langmuir*, *26*(13), 11041–11049. https://doi.org/10.1021/la1005242
1245 Dimova, R. (2019). Giant Vesicles and Their Use in Assays for Assessing Membrane Phase State,
1246 Curvature, Mechanics, and Electrical Properties. *Annual Review of Biophysics*, *48*(1),
1247 93–119. https://doi.org/10.1146/annurev-biophys-052118-115342
1248 Doktorova, M., Heberle, F. A., Eicher, B., Standaert, R. F., Katsaras, J., London, E., Pabst, G., &
1249 Marquardt, D. (2018). Preparation of asymmetric phospholipid vesicles for use as cell

membrane models. *Nature Protocols*, *13*(9), 2086–2101. https://doi.org/10.1038/s41596-018-0033-6

Domenech, O., Redondo, L., Picas, L., Morros, A., Montero, M. T., & Hernandez-Borrell, J. (2007). Atomic force microscopy characterization of supported planar bilayers that mimic the mitochondrial inner membrane. *Journal of Molecular Recognition*, *20*(6), 546–553. https://doi.org/10.1002/jmr.849

Dufrêne, Y. F., Ando, T., Garcia, R., Alsteens, D., Martinez-Martin, D., Engel, A., Gerber, C., & Müller, D. J. (2017). Imaging modes of atomic force microscopy for application in molecular and cell biology. *Nature Nanotechnology*, *12*, 295. https://doi.org/10.1038/nnano.2017.45

Dufrene, Y. F., Barger, W. R., Green, J. B. D., & Lee, G. U. (1997). Nanometer-scale surface properties of mixed phospholipid monolayers and bilayers. *Langmuir*, *13*(18), 4779–4784. https://doi.org/10.1021/la970221r

Dufrene, Y. F., Boland, T., Schneider, J. W., Barger, W. R., & Lee, G. U. (1998). Characterization of the physical properties of model biomembranes at the nanometer scale with the atomic force microscope. *Faraday Discussions*, *111*, 79–94.

Dufrêne, Y. F., & Lee, G. U. (2000). Advances in the characterization of supported lipid films with the atomic force microscope. *Biochimica et Biophysica Acta (BBA) - Biomembranes*, *1509*(1), 14–41. https://doi.org/10.1016/S0005-2736(00)00346-1

Ehrig, J., Petrov, E. P., & Schwille, P. (2011). Phase separation and near-critical fluctuations in two-component lipid membranes: Monte Carlo simulations on experimentally relevant scales. *New Journal of Physics*, *13*(4), 045019. https://doi.org/10.1088/1367-2630/13/4/045019

El Kirat, K., Morandat, S., & Dufrene, Y. F. (2010). Nanoscale analysis of supported lipid bilayers using atomic force microscopy. *Biochimica Et Biophysica Acta-Biomembranes*, *1798*(4), 750–765. https://doi.org/10.1016/j.bbamem.2009.07.026

1276 Evans, E, & Ritchie, K. (1997). Dynamic strength of molecular adhesion bonds. *Biophysical*
1277 *Journal*, *72*(4), 1541–1555.
1278 Evans, E, & Yeung, A. (1994). Hidden dynamics in rapid changes of bilayer shape. *Chemistry and*
1279 *Physics of Lipids*, *73*(1), 39–56. https://doi.org/10.1016/0009-3084(94)90173-2
1280 Evans, Evan, Heinrich, V., Ludwig, F., & Rawicz, W. (2003). Dynamic Tension Spectroscopy and
1281 Strength of Biomembranes. *Biophysical Journal*, *85*(4), 2342–2350.
1282 Fidorra, M., Heimburg, T., & Seeger, H. M. (2009). Melting of individual lipid components in
1283 binary lipid mixtures studied by FTIR spectroscopy, DSC and Monte Carlo simulations.
1284 *Biochimica Et Biophysica Acta-Biomembranes*, *1788*(3), 600–607.
1285 https://doi.org/10.1016/j.bbamem.2008.12.003
1286 Florin, E. L., Moy, V. T., & Gaub, H. E. (1994). Adhesion forces between individual ligand-
1287 receptor pairs. *Science*, *264*(5157), 415 LP – 417.
1288 https://doi.org/10.1126/science.8153628
1289 Franz, V., Loi, S., Muller, H., Bamberg, E., & Butt, H. H. (2002). Tip penetration through lipid
1290 bilayers in atomic force microscopy. *Colloids and Surfaces B-Biointerfaces*, *23*(2–3),
1291 191–200.
1292 García-Arribas, A. B., Alonso, A., & Goñi, F. M. (2016). Cholesterol interactions with ceramide
1293 and sphingomyelin. *Chemistry and Physics of Lipids*, *199*, 26–34.
1294 https://doi.org/10.1016/j.chemphyslip.2016.04.002
1295 García-Arribas, A. B., González-Ramírez, E. J., Sot, J., Areso, I., Alonso, A., & Goñi, F. M. (2017).
1296 Complex Effects of 24:1 Sphingolipids in Membranes Containing
1297 Dioleoylphosphatidylcholine and Cholesterol. *Langmuir*, *33*(22), 5545–5554.
1298 https://doi.org/10.1021/acs.langmuir.7b00162
1299 Garcia-Manyes, S, Guell, A. G., Gorostiza, P., & Sanz, F. (2005). Nanomechanics of silicon
1300 surfaces with atomic force microscopy: An insight to the first stages of plastic
1301 deformation. *Journal of Chemical Physics*, *123*(11). https://doi.org/10.1063/1.2035094

1302 Garcia-Manyes, S, Oncins, G., & Sanz, F. (2005a). Effect of ion-binding and chemical
1303 phospholipid structure on the nanomechanics of lipid bilayers studied by force
1304 spectroscopy. *Biophysical Journal*, *89*, 1812–1826.
1305 https://doi.org/10.1529/biophysj.105.064030
1306 Garcia-Manyes, S, Oncins, G., & Sanz, F. (2005b). Effect of temperature on the nanomechanics
1307 of lipid bilayers studied by force spectroscopy. *Biophysical Journal*, *89*(6), 4261–4274.
1308 https://doi.org/10.1529/biophysj.105.065581
1309 Garcia-Manyes, S, Redondo-Morata, L., Oncins, G., & Sanz, F. (2010). Nanomechanics of Lipid
1310 Bilayers: Heads or Tails? *Journal of the American Chemical Society*, *132*(37), 12874–
1311 12886. https://doi.org/10.1021/ja1002185
1312 Garcia-Manyes, S, & Sanz, F. (2010). Nanomechanics of lipid bilayers by force spectroscopy
1313 with AFM: A perspective. *Biochimica Et Biophysica Acta-Biomembranes*, *1798*(4), 741–
1314 749. https://doi.org/10.1016/j.bbamem.2009.12.019
1315 Garcia-Manyes, Sergi, Redondo-Morata, L., Oncins, G., & Sanz, F. (2010). Nanomechanics of
1316 Lipid Bilayers: Heads or Tails? *Journal of the American Chemical Society*, *132*(37),
1317 12874–12886. https://doi.org/10.1021/ja1002185
1318 Giannotti, M. I., & Vancso, G. J. (2007). Interrogation of single synthetic polymer chains and
1319 polysaccharides by AFM-based force spectroscopy. *ChemPhysChem*, *8*(16).
1320 https://doi.org/10.1002/cphc.200700175
1321 Giles, R., Cleveland, J. P., Manne, S., Hansma, P. K., Drake, B., Maivald, P., Boles, C., Gurley, J.,
1322 & Elings, V. (1993). Noncontact force microscopy in liquids. *Applied Physics Letters*,
1323 *63*(5), 617–618. https://doi.org/10.1063/1.109967
1324 Gillissen, J. J. J., Jackman, J. A., Tabaei, S. R., Yoon, B. K., & Cho, N.-J. (2017). Quartz Crystal
1325 Microbalance Model for Quantitatively Probing the Deformation of Adsorbed Particles
1326 at Low Surface Coverage. *Analytical Chemistry*, *89*(21), 11711–11718.
1327 https://doi.org/10.1021/acs.analchem.7b03179

1328 Goñi, F. M. (2019a). “Rafts”: A nickname for putative transient nanodomains. *Chemistry and*
1329 *Physics of Lipids*, *218*, 34–39. https://doi.org/10.1016/j.chemphyslip.2018.11.006
1330 Goñi, F. M. (2019b). “Rafts”: A nickname for putative transient nanodomains. In *Chemistry and*
1331 *Physics of Lipids* (Vol. 218, pp. 34–39). Elsevier Ireland Ltd.
1332 https://doi.org/10.1016/j.chemphyslip.2018.11.006
1333 González-Ramírez, E. J., Artetxe, I., García-Arribas, A. B., Goñi, F. M., & Alonso, A. (2019).
1334 Homogeneous and Heterogeneous Bilayers of Ternary Lipid Compositions Containing
1335 Equimolar Ceramide and Cholesterol. *Langmuir*, *35*(15), 5305–5315.
1336 https://doi.org/10.1021/acs.langmuir.9b00324
1337 Gumí-Audenis, B., Costa, L., Carlá, F., Comin, F., Sanz, F., & Giannotti, M. I. (2016a). Structure
1338 and nanomechanics of model membranes by atomic force microscopy and
1339 spectroscopy: Insights into the role of cholesterol and sphingolipids. *Membranes*, *6*(4).
1340 https://doi.org/10.3390/membranes6040058
1341 Gumí-Audenis, B., Costa, L., Carlá, F., Comin, F., Sanz, F., & Giannotti, M. I. (2016b). Structure
1342 and nanomechanics of model membranes by atomic force microscopy and
1343 spectroscopy: Insights into the role of cholesterol and sphingolipids. *Membranes*, *6*(4).
1344 https://doi.org/10.3390/membranes6040058
1345 Gumí-Audenis, B., Costa, L., Redondo-Morata, L., Milhiet, P.-E., Sanz, F., Felici, R., Giannotti, M.
1346 I., & Carlà, F. (2018). In-plane molecular organization of hydrated single lipid bilayers:
1347 DPPC: cholesterol. *Nanoscale*, *10*(1). https://doi.org/10.1039/c7nr07510c
1348 Gumi-Audenis, B., Costa, L., Redondo-Morata, L., Milhiet, P.-E., Sanz, F., Felici, R., Giannotti, M.
1349 I., & Carla, F. (2018). In-plane molecular organization of hydrated single lipid bilayers:
1350 DPPC:cholesterol. *Nanoscale*, *10*(1), 87–92. https://doi.org/10.1039/c7nr07510c
1351 Gumí-Audenis, Berta, Costa, L., Ferrer-Tasies, L., Ratera, I., Ventosa, N., Sanz, F., & Giannotti,
1352 M. I. (2018). Pulling lipid tubes from supported bilayers unveils the underlying

substrate contribution to the membrane mechanics. *Nanoscale*. https://doi.org/10.1039/C8NR03249A

Gumí-Audenis, Berta, Sanz, F., & Giannotti, M. I. (2015). Impact of galactosylceramides on the nanomechanical properties of lipid bilayer models: An AFM-force spectroscopy study. *Soft Matter*, *11*(27), 5447–5454. https://doi.org/10.1039/C5SM01252J

Guyomarc'h, F., Zou, S., Chen, M., Milhiet, P.-E., Godefroy, C., Vié, V., & Lopez, C. (2014). Milk Sphingomyelin Domains in Biomimetic Membranes and the Role of Cholesterol: Morphology and Nanomechanical Properties Investigated Using AFM and Force Spectroscopy. *Langmuir*, *30*(22), 6516–6524. https://doi.org/10.1021/la501640y

Hardy, G. J., Nayak, R., & Zauscher, S. (2013). Model cell membranes: Techniques to form complex biomimetic supported lipid bilayers via vesicle fusion. *Current Opinion in Colloid & Interface Science*, *18*(5), 448–458. https://doi.org/10.1016/j.cocis.2013.06.004

Hasan, I. Y., & Mechler, A. (2015). Viscoelastic changes measured in partially suspended single bilayer membranes. *Soft Matter*, *11*(27), 5571–5579. https://doi.org/10.1039/C5SM00278H

Hassinger, J. E., Oster, G., Drubin, D. G., & Rangamani, P. (2017). Design principles for robust vesiculation in clathrin-mediated endocytosis. *Proceedings of the National Academy of Sciences*, *114*(7), E1118 LP-E1127. https://doi.org/10.1073/pnas.1617705114

Heimburg, T. (1998). Mechanical aspects of membrane thermodynamics. Estimation of the mechanical properties of lipid membranes close to the chain melting transition from calorimetry. *Biochimica Et Biophysica Acta-Biomembranes*, *1415*(1), 147–162. https://doi.org/10.1016/s0005-2736(98)00189-8

Hill, T. L. (2013). *Thermodynamics of Small Systems/* (Reprint). Dover Publications Inc.

1377 Hochmuth, F. M., Shao, J. Y., Dai, J., & Sheetz, M. P. (1996). Deformation and flow of
1378 membrane into tethers extracted from neuronal growth cones. *Biophysical Journal*,
1379 *70*(1), 358–369.
1380 Hohner, A. O., David, M. P. C., & Rädler, J. O. (2010). Controlled solvent-exchange deposition of
1381 phospholipid membranes onto solid surfaces. *Biointerphases*, *5*(1), 1–8.
1382 https://doi.org/10.1116/1.3319326
1383 Hugel, T., & Seitz, M. (2001). The Study of Molecular Interactions by AFM Force Spectroscopy.
1384 *Macromolecular Rapid Communications*, *22*(13), 989–1016.
1385 https://doi.org/10.1002/1521-3927(20010901)22:13<989::AID-MARC989>3.0.CO;2-D
1386 Hung, W.-C., Lee, M.-T., Chen, F.-Y., & Huang, H. W. (2007). The condensing effect of
1387 cholesterol in lipid bilayers. *Biophysical Journal*, *92*(11), 3960–3967.
1388 https://doi.org/10.1529/biophysj.106.099234
1389 Hurley, J. H., Boura, E., Carlson, L.-A., & Rózycki, B. (2010). Membrane Budding. *Cell*, *143*(6),
1390 875–887. https://doi.org/10.1016/j.cell.2010.11.030
1391 Ira, Zou, S., Ramirez, D. M. C., Vanderlip, S., Ogilvie, W., Jakubek, Z. J., & Johnston, L. J. (2009).
1392 Enzymatic generation of ceramide induces membrane restructuring: Correlated AFM
1393 and fluorescence imaging of supported bilayers. *Journal of Structural Biology*, *168*(1),
1394 78–89. https://doi.org/10.1016/j.jsb.2009.03.014
1395 Jiménez-Rojo, N., García-Arribas, A. B., Sot, J., Alonso, A., & Goñi, F. M. (2014). Lipid bilayers
1396 containing sphingomyelins and ceramides of varying N-acyl lengths: A glimpse into
1397 sphingolipid complexity. *Biochimica et Biophysica Acta - Biomembranes*, *1838*(1
1398 PARTB), 456–464. https://doi.org/10.1016/j.bbamem.2013.10.010
1399 Jing, Y., Trefna, H., Persson, M., Kasemo, B., & Svedhem, S. (2013). Formation of supported
1400 lipid bilayers on silica: Relation to lipid phase transition temperature and liposome
1401 size. *Soft Matter*, *10*(1), 187–195. https://doi.org/10.1039/C3SM50947H

1402 Johnston, L. J. (2007). Nanoscale imaging of domains in supported lipid membranes. *Langmuir:*
1403 *The ACS Journal of Surfaces and Colloids*, *23*(11), 5886–5895.
1404 https://doi.org/10.1021/la070108t
1405 Kahya, N., Scherfeld, D., Bacia, K., & Schwille, P. (2004). Lipid domain formation and dynamics
1406 in giant unilamellar vesicles explored by fluorescence correlation spectroscopy. *Journal*
1407 *of Structural Biology*, *147*(1), 77–89. https://doi.org/10.1016/j.jsb.2003.09.021
1408 Kechagia, J. Z., Ivaska, J., & Roca-Cusachs, P. (2019). Integrins as biomechanical sensors of the
1409 microenvironment. *Nature Reviews Molecular Cell Biology*, *20*(8), 457–473.
1410 https://doi.org/10.1038/s41580-019-0134-2
1411 Keller, C. A., & Kasemo, B. (1998). Surface specific kinetics of lipid vesicle adsorption measured
1412 with a quartz crystal microbalance. *Biophysical Journal*, *75*(3), 1397–1402.
1413 Keller, D., Larsen, N. B., Moller, I. M., & Mouritsen, O. G. (2005). Decoupled phase transitions
1414 and grain-boundary melting in supported phospholipid bilayers. *Physical Review*
1415 *Letters*, *94*(2). https://doi.org/10.1103/PhysRevLett.94.025701
1416 Kodera, N., Yamamoto, D., Ishikawa, R., & Ando, T. (2010). Video imaging of walking myosin V
1417 by high-speed atomic force microscopy. *Nature*, *468*(7320).
1418 https://doi.org/10.1038/nature09450
1419 Kurniawan, J., Ventrici de Souza, J. F., Dang, A. T., Liu, G., & Kuhl, T. L. (2018). Preparation and
1420 Characterization of Solid-Supported Lipid Bilayers Formed by Langmuir–Blodgett
1421 Deposition: A Tutorial. *Langmuir*, *34*(51), 15622–15639.
1422 https://doi.org/10.1021/acs.langmuir.8b03504
1423 Lee, G. U., Chrisey, L. A., & Colton, R. J. (1994). DIRECT MEASUREMENT OF THE FORCES
1424 BETWEEN COMPLEMENTARY STRANDS OF DNA. *Science*, *266*(5186), 771–773.
1425 https://doi.org/10.1126/science.7973628
1426 Leonenko, Z. V, Finot, E., Ma, H., Dahms, T. E. S., & Cramb, D. T. (2004). Investigation of
1427 temperature-induced phase transitions in DOPC and DPPC phospholipid bilayers using

1428 temperature-controlled scanning force microscopy. *Biophysical Journal*, *86*(6), 3783–
1429 3793. https://doi.org/10.1529/biophysj.103.036681
1430 Leonenko, Z. V., Finot, E., Ma, H., Dahms, T. E. S., & Cramb, D. T. (2004). Investigation of
1431 temperature-induced phase transitions in DOPC and DPPC phospholipid bilayers using
1432 temperature-controlled scanning force microscopy. *Biophysical Journal*, *86*(6), 3783–
1433 3793. https://doi.org/10.1529/biophysj.103.036681
1434 Lin, D. C., Dimitriadis, E. K., & Horkay, F. (2007). Robust strategies for automated AFM force
1435 curve analysis—I. Non-adhesive indentation of soft, inhomogeneous materials. *Journal*
1436 *of Biomechanical Engineering*, *129*(3), 430–440. https://doi.org/10.1115/1.2720924
1437 Lin, W.-C., Blanchette, C. D., & Longo, M. L. (2007). Fluid-Phase Chain Unsaturation Controlling
1438 Domain Microstructure and Phase in Ternary Lipid Bilayers Containing GalCer and
1439 Cholesterol. *Biophysical Journal*, *92*(8), 2831–2841.
1440 https://doi.org/10.1529/biophysj.106.095422
1441 Lind, T. K., & Cárdenas, M. (2016). Understanding the formation of supported lipid bilayers via
1442 vesicle fusion-A case that exemplifies the need for the complementary method
1443 approach (Review). *Biointerphases*, *11*(2), 020801. https://doi.org/10.1116/1.4944830
1444 Lipowsky, R., & Seifert, U. (1991). Adhesion of Vesicles and Membranes. *Molecular Crystals*
1445 *and Liquid Crystals*, *202*(1), 17–25. https://doi.org/10.1080/00268949108035656
1446 Loi, S, Sun, G., Franz, V., & Butt, H. J. (2002). Rupture of molecular thin films observed in
1447 atomic force microscopy. II. Experiment. *Physical Review E*, *66*(3).
1448 https://doi.org/031602 10.1103/PhysRevE.66.031602
1449 Loi, Simona, Sun, G., Franz, V., & Butt, H.-J. (2002). Rupture of molecular thin films observed in
1450 atomic force microscopy. II. Experiment. *Phys Rev E Stat Nonlin Soft Matter Phys*, *66*(3
1451 Pt 1), 31602.
1452 Losada-Pérez, P., Jiménez-Monroy, K. L., Grinsven, B. van, Leys, J., Janssens, S. D., Peeters, M.,
1453 Glorieux, C., Thoen, J., Haenen, K., Ceuninck, W. D., & Wagner, P. (2014). Phase

transitions in lipid vesicles detected by a complementary set of methods: Heat-transfer measurements, adiabatic scanning calorimetry, and dissipation-mode quartz crystal microbalance. *Physica Status Solidi (a)*, *211*(6), 1377–1388. https://doi.org/10.1002/pssa.201431060

Losada-Pérez, P., Khorshid, M., Yongabi, D., & Wagner, P. (2015). Effect of Cholesterol on the Phase Behavior of Solid-Supported Lipid Vesicle Layers. *The Journal of Physical Chemistry B*, *119*(15), 4985–4992. https://doi.org/10.1021/acs.jpcb.5b00712

Losada-Pérez, P., Mertens, N., de Medio-Vasconcelos, B., Slenders, E., Leys, J., Peeters, M., van Grinsven, B., Gruber, J., Glorieux, C., Pfeiffer, H., Wagner, P., & Thoen, J. (2015). *Phase Transitions of Binary Lipid Mixtures: A Combined Study by Adiabatic Scanning Calorimetry and Quartz Crystal Microbalance with Dissipation Monitoring* [Research Article]. Advances in Condensed Matter Physics; Hindawi. https://doi.org/10.1155/2015/479318

Mabrey, S., & Sturtevant, J. M. (1976). Investigation of phase transitions of lipids and lipid mixtures by high sensitivity differential scanning calorimetry. *Proceedings of the National Academy of Sciences of the United States of America*, *73*(11), 3862–3866. https://doi.org/10.1073/pnas.73.11.3862

Maeda, N., Senden, T. J., & di Meglio, J.-M. (2002). Micromanipulation of phospholipid bilayers by atomic force microscopy. *Biochimica et Biophysica Acta (BBA) - Biomembranes*, *1564*(1), 165–172.

Mannock, D. A., Lewis, R. N. A. H., & McElhaney, R. N. (2010). A calorimetric and spectroscopic comparison of the effects of ergosterol and cholesterol on the thermotropic phase behavior and organization of dipalmitoylphosphatidylcholine bilayer membranes. *Biochimica Et Biophysica Acta*, *1798*(3), 376–388. https://doi.org/10.1016/j.bbamem.2009.09.002

1479 Marcus, W. D., & Hochmuth, R. M. (2002). Experimental Studies of Membrane Tethers Formed
1480 from Human Neutrophils. *Annals of Biomedical Engineering*, *30*(10), 1273–1280.
1481 https://doi.org/10.1114/1.1528614
1482 Marszalek, P E, Lu, H., Li, H. B., Carrion-Vazquez, M., Oberhauser, A. F., Schulten, K., &
1483 Fernandez, J. M. (1999). Mechanical unfolding intermediates in titin modules. *Nature*,
1484 *402*(6757), 100–103.
1485 Marszalek, Piotr E, Li, H., & Fernandez, J. M. (2001). Fingerprinting polysaccharides with single-
1486 molecule atomic force microscopy. *Nat Biotech*, *19*(3), 258–262.
1487 Mennicke, U., & Salditt, T. (2002). Preparation of solid-supported lipid bilayers by spin-coating.
1488 *Langmuir*, *18*(21), 8172–8177. https://doi.org/10.1021/la025863f
1489 Mierzwa, B. E., Chiaruttini, N., Redondo-Morata, L., von Filseck, J. M., Koenig, J., Larios, J.,
1490 Poser, I., Mueller-Reichert, T., Scheuring, S., Roux, A., & Gerlich, D. W. (2017). Dynamic
1491 subunit turnover in ESCRT-III assemblies is regulated by Vps4 to mediate membrane
1492 remodelling during cytokinesis. *Nature Cell Biology*, *19*(7), 787-+.
1493 https://doi.org/10.1038/ncb3559
1494 Mills, T. T., Huang, J., Feigenson, G. W., & Nagle, J. F. (2009). Effects of cholesterol and
1495 unsaturated DOPC lipid on chain packing of saturated gel-phase DPPC bilayers. *General*
1496 *Physiology and Biophysics*, *28*(2), 126–139.
1497 Mingeot-Leclercq, M. P., Deleu, M., Brasseur, R., & Dufrene, Y. F. (2008). Atomic force
1498 microscopy of supported lipid bilayers. *Nature Protocols*, *3*(10), 1654–1659.
1499 https://doi.org/10.1038/nprot.2008.149
1500 Miyoshi, T., Lönnfors, M., Peter Slotte, J., & Kato, S. (2014). A detailed analysis of partial
1501 molecular volumes in DPPC/cholesterol binary bilayers. *Biochimica Et Biophysica Acta*,
1502 *1838*(12), 3069–3077. https://doi.org/10.1016/j.bbamem.2014.07.004

1503 Morandat, S., Azouzi, S., Beauvais, E., Mastouri, A., & El Kirat, K. (2013). Atomic force
1504 microscopy of model lipid membranes. *Analytical and Bioanalytical Chemistry*, *405*(5),
1505 1445–1461. https://doi.org/10.1007/s00216-012-6383-y
1506 Mouritsen, O. G., & Bloom, M. (1984). MATTRESS MODEL OF LIPID-PROTEIN INTERACTIONS IN
1507 MEMBRANES. *Biophysical Journal*, *46*(2), 141–153.
1508 Nagle, J. F., & Tristram-Nagle, S. (2000). Structure of lipid bilayers. *Biochimica Et Biophysica*
1509 *Acta-Reviews on Biomembranes*, *1469*(3), 159–195. https://doi.org/10.1016/s0304-
1510 4157(00)00016-2
1511 Nawaz, S., Sánchez, P., Schmitt, S., Snaidero, N., Mitkovski, M., Velte, C., Brückner, B. R.,
1512 Alexopoulos, I., Czopka, T., Jung, S. Y., Rhee, J. S., Janshoff, A., Witke, W., Schaap, I. A.
1513 T., Lyons, D. A., & Simons, M. (2015). Actin Filament Turnover Drives Leading Edge
1514 Growth during Myelin Sheath Formation in the Central Nervous System.
1515 *Developmental Cell*, *34*(2), 139–151. https://doi.org/10.1016/j.devcel.2015.05.013
1516 Neupane, S., De Smet, Y., Renner, F. U., & Losada-Pérez, P. (2018). Quartz Crystal Microbalance
1517 With Dissipation Monitoring: A Versatile Tool to Monitor Phase Transitions in
1518 Biomimetic Membranes. *Frontiers in Materials*, *5*.
1519 https://doi.org/10.3389/fmats.2018.00046
1520 Noy, A., Vezenov, D. V, & Lieber, C. M. (1997). CHEMICAL FORCE MICROSCOPY. *Annual Review*
1521 *of Materials Science*, *27*(1), 381–421.
1522 https://doi.org/10.1146/annurev.matsci.27.1.381
1523 Olsson, A. L. J., Quevedo, I. R., He, D., Basnet, M., & Tufenkji, N. (2013). Using the Quartz
1524 Crystal Microbalance with Dissipation Monitoring to Evaluate the Size of Nanoparticles
1525 Deposited on Surfaces. *ACS Nano*, *7*(9), 7833–7843.
1526 https://doi.org/10.1021/nn402758w

1527 Pan, J., Mills, T. T., Tristram-Nagle, S., & Nagle, J. F. (2008). Cholesterol perturbs lipid bilayers
1528 nonuniversally. *Physical Review Letters*, *100*(19), 198103.
1529 https://doi.org/10.1103/PhysRevLett.100.198103
1530 Parot, P., Dufrêne, Y. F., Hinterdorfer, P., Le Grimellec, C., Navajas, D., Pellequer, J. L., &
1531 Scheuring, S. (2007). Past, present and future of atomic force microscopy in life
1532 sciences and medicine. *J Mol Recognit*, *20*(6), 418–431.
1533 https://doi.org/10.1002/jmr.857
1534 Peschel, A., Langhoff, A., Uhl, E., Dathathreyan, A., Haindl, S., Johannsmann, D., & Reviakine, I.
1535 (2016). Lipid phase behavior studied with a quartz crystal microbalance: A technique
1536 for biophysical studies with applications in screening. *The Journal of Chemical Physics*,
1537 *145*(20), 204904. https://doi.org/10.1063/1.4968215
1538 Picas, L., Montero, M. T., Morros, A., Cabanas, M. E., Seantier, B., Milhiet, P.-E., & Hernandez-
1539 Borrell, J. (2009). Calcium-Induced Formation of Subdomains in
1540 Phosphatidylethanolamine-Phosphatidylglycerol Bilayers: A Combined DSC, (31)P
1541 NMR, and AFM Study. *Journal of Physical Chemistry B*, *113*(14), 4648–4655.
1542 https://doi.org/10.1021/jp8102468
1543 Picas, L., Rico, F., & Scheuring, S. (2012). Direct Measurement of the Mechanical Properties of
1544 Lipid Phases in Supported Bilayers. *Biophysical Journal*, *102*(1), L1–L3.
1545 https://doi.org/10.1016/j.bpj.2011.11.4001
1546 Piggot, T. J., Allison, J. R., Sessions, R. B., & Essex, J. W. (2017). On the Calculation of Acyl Chain
1547 Order Parameters from Lipid Simulations. *Journal of Chemical Theory and*
1548 *Computation*, *13*(11), 5683–5696. https://doi.org/10.1021/acs.jctc.7b00643
1549 Pinkwart, K., Schneider, F., Lukoseviciute, M., Sauka-Spengler, T., Lyman, E., Eggeling, C., &
1550 Sezgin, E. (2019). Nanoscale dynamics of cholesterol in the cell membrane. *Journal of*
1551 *Biological Chemistry*, *294*(34), 12599–12609.
1552 https://doi.org/10.1074/jbc.RA119.009683

1553 Pramanik, S. K., Seneca, S., Ethirajan, A., Neupane, S., Renner, F. U., & Losada-Pérez, P. (2016).
1554 Ionic strength dependent vesicle adsorption and phase behavior of anionic
1555 phospholipids on a gold substrate. *Biointerphases*, *11*(1), 019006.
1556 https://doi.org/10.1116/1.4939596
1557 Radmacher, M. (1997). Measuring the elastic properties of biological samples with the AFM.
1558 *IEEE Engineering in Medicine and Biology Magazine*, *16*(2), 47–57.
1559 https://doi.org/10.1109/51.582176
1560 Rascol, E., Devoisselle, J.-M., & Chopineau, J. (2016). The relevance of membrane models to
1561 understand nanoparticles–cell membrane interactions. *Nanoscale*, *8*(9), 4780–4798.
1562 https://doi.org/10.1039/C5NR07954C
1563 Rawicz, W., Olbrich, K. C., McIntosh, T., Needham, D., & Evans, E. (2000). Effect of chain length
1564 and unsaturation on elasticity of lipid bilayers. *Biophysical Journal*, *79*(1), 328–339.
1565 Redondo-Morata, L, Giannotti, M. I., & Sanz, F. (2012a). AFM-Based Force-Clamp Monitors
1566 Lipid Bilayer Failure Kinetics. *Langmuir*, *28*(15), 6403–6410.
1567 https://doi.org/10.1021/la3005147
1568 Redondo-Morata, L, Giannotti, M. I., & Sanz, F. (2012b). Influence of Cholesterol on the Phase
1569 Transition of Lipid Bilayers: A Temperature-Controlled Force Spectroscopy Study.
1570 *Langmuir*, *28*(35), 12851–12860. https://doi.org/10.1021/la302620t
1571 Redondo-Morata, L, Giannotti, M. I., & Sanz, F. (2012c). Influence of Cholesterol on the Phase
1572 Transition of Lipid Bilayers: A Temperature-Controlled Force Spectroscopy Study.
1573 *Langmuir*, *28*(35), 12851–12860. https://doi.org/10.1021/la302620t
1574 Redondo-Morata, L., Giannotti, M. I., & Sanz, F. (2012). Stability of Lipid Bilayers as Model
1575 Membranes: Atomic Force Microscopy and Spectroscopy Approach. In *Atomic Force*
1576 *Microscopy in Liquid: Biological Applications*.
1577 https://doi.org/10.1002/9783527649808.ch10

1578 Redondo-Morata, L, Giannotti, M. I., & Sanz, F. (2014). Structural impact of cations on lipid
1579 bilayer models: Nanomechanical properties by AFM-force spectroscopy. *Molecular*
1580 *Membrane Biology*, *31*(1), 17–28. https://doi.org/10.3109/09687688.2013.868940
1581 Redondo-Morata, L, Sanford, R. L., Andersen, O. S., & Scheuring, S. (2016). Effect of Statins on
1582 the Nanomechanical Properties of Supported Lipid Bilayers. *Biophysical Journal*,
1583 *111*(2), 363–372. https://doi.org/10.1016/j.bpj.2016.06.016
1584 Redondo-Morata, Lorena, Oncins, G., & Sanz, F. (2012). Force Spectroscopy Reveals the Effect
1585 of Different Ions in the Nanomechanical Behavior of Phospholipid Model Membranes:
1586 The Case of Potassium Cation. *Biophysical Journal*, *102*(1), 66–74.
1587 https://doi.org/10.1016/j.bpj.2011.10.051
1588 Reimhult, E., Hook, F., & Kasemo, B. (2003). Intact vesicle adsorption and supported
1589 biomembrane formation from vesicles in solution: Influence of surface chemistry,
1590 vesicle size, temperature, and osmotic pressure. *Langmuir*, *19*(5), 1681–1691.
1591 https://doi.org/10.1021/la0263920
1592 Relat-Goberna, J., Beedle Amy, E. M., & Garcia-Manyes, S. (2017). The Nanomechanics of Lipid
1593 Multibilayer Stacks Exhibits Complex Dynamics. *Small*, *13*(24), 1700147.
1594 https://doi.org/10.1002/smll.201700147
1595 Reviakine, I., Gallego, M., Johannsmann, D., & Tellechea, E. (2012). Adsorbed liposome
1596 deformation studied with quartz crystal microbalance. *The Journal of Chemical Physics*,
1597 *136*(8), 084702. https://doi.org/10.1063/1.3687351
1598 Reviakine, I., Johannsmann, D., & Richter, R. P. (2011). Hearing What You Cannot See and
1599 Visualizing What You Hear: Interpreting Quartz Crystal Microbalance Data from
1600 Solvated Interfaces. *Analytical Chemistry*, *83*(23), 8838–8848.
1601 https://doi.org/10.1021/ac201778h

1602 Richter, R., Mukhopadhyay, A., & Brisson, A. (2003). Pathways of Lipid Vesicle Deposition on
1603 Solid Surfaces: A Combined QCM-D and AFM Study. *Biophysical Journal*, *85*(5), 3035–
1604 3047.
1605 Richter, R P. (2006). Formation of solid-supported lipid bilayers: An integrated view. *Langmuir*,
1606 *22*(8), 3497–3505. https://doi.org/10.1021/la052687c
1607 Richter, Ralf P, & Brisson, A. (2003). Characterization of Lipid Bilayers and Protein Assemblies
1608 Supported on Rough Surfaces by Atomic Force Microscopy. *Langmuir*, *19*(5), 1632–
1609 1640. https://doi.org/10.1021/la026427w
1610 Richter, Ralf P, & Brisson, A. R. (2005). Following the Formation of Supported Lipid Bilayers on
1611 Mica: A Study Combining AFM, QCM-D, and Ellipsometry. *Biophysical Journal*, *88*(5),
1612 3422–3433. https://doi.org/10.1529/biophysj.104.053728
1613 Rief, M., Oesterhelt, F., Heymann, B., & Gaub, H. E. (1997). Single Molecule Force Spectroscopy
1614 on Polysaccharides by Atomic Force Microscopy. *Science*, *275*(5304), 1295 LP – 1297.
1615 https://doi.org/10.1126/science.275.5304.1295
1616 Rog, T., Pasenkiewicz-Gierula, M., Vattulainen, I., & Karttunen, M. (2009). Ordering effects of
1617 cholesterol and its analogues. *Biochimica Et Biophysica Acta-Biomembranes*, *1788*(1),
1618 97–121. https://doi.org/10.1016/j.bbamem.2008.08.022
1619 Roux, A. (2013). The physics of membrane tubes: Soft templates for studying cellular
1620 membranes. *Soft Matter*, *9*(29), 6726–6736.
1621 Sauerbrey, G. (1959). Verwendung von Schwingquarzen zur Wägung dünner Schichten und zur
1622 Mikrowägung. *Zeitschrift für Physik*, *155*(2), 206–222.
1623 https://doi.org/10.1007/BF01337937
1624 Schmidtke, D. W., & Diamond, S. L. (2000). Direct Observation of Membrane Tethers Formed
1625 during Neutrophil Attachment to Platelets or P-Selectin under Physiological Flow. *The*
1626 *Journal of Cell Biology*, *149*(3), 719.

1627 Schneider, J., Dufrene, Y. F., Barger, W. R., & Lee, G. U. (2000). Atomic force microscope image
1628 contrast mechanisms on supported lipid bilayers. *Biophysical Journal*, *79*(2), 1107–
1629 1118.
1630 Sebaaly, C., Greige-Gerges, H., & Charcosset, C. (2019). *Chapter 11—Lipid Membrane Models*
1631 *for Biomembrane Properties' Investigation* (A. Basile & C. B. T.-C. T. and F. D. on (Bio-)
1632 M. Charcosset, Eds.; pp. 311–340). Elsevier. https://doi.org/10.1016/B978-0-12-
1633 813606-5.00011-7
1634 Seeger, H. M., Di Cerbo, A., Alessandrini, A., & Facci, P. (2010). Supported Lipid Bilayers on
1635 Mica and Silicon Oxide: Comparison of the Main Phase Transition Behavior. *Journal of*
1636 *Physical Chemistry B*, *114*(27), 8926–8933. https://doi.org/10.1021/jp1026477
1637 Sessa, G., & Weissmann, G. (1968). Phospholipid spherules (liposomes) as a model for
1638 biological membranes. *Journal of Lipid Research*, *9*(3), 310–318.
1639 Shao, J.-Y., Ting-Beall, H. P., & Hochmuth, R. M. (1998). Static and dynamic lengths of
1640 neutrophil microvilli. *Proceedings of the National Academy of Sciences*, *95*(12), 6797.
1641 Sheetz, M. P. (2001). Cell control by membrane-cytoskeleton adhesion. *Nature Reviews*
1642 *Molecular Cell Biology*, *2*, 392.
1643 Shinoda, K., Shinoda, W., & Mikami, M. (2007). Molecular dynamics simulation of an archaeal
1644 lipid bilayer with sodium chloride. *Physical Chemistry Chemical Physics*, *9*(5), 643–650.
1645 https://doi.org/10.1039/b611543h
1646 Simons, K., & Ikonen, E. (1997). Functional rafts in cell membranes. *Nature*, *387*(6633), 569–
1647 572. https://doi.org/10.1038/42408
1648 Singer, S. J., & Nicolson, G. L. (1972). FLUID MOSAIC MODEL OF STRUCTURE OF CELL-
1649 MEMBRANES. *Science*, *175*(4023), 720-. https://doi.org/10.1126/science.175.4023.720
1650 Siontorou, C. G., Nikoleli, G.-P., Nikolelis, D. P., & Karapetis, S. K. (2017). Artificial Lipid
1651 Membranes: Past, Present, and Future. *Membranes*, *7*(3), 38.
1652 https://doi.org/10.3390/membranes7030038

1653 Steinkühler, J., Sezgin, E., Urbančič, I., Eggeling, C., & Dimova, R. (2019). Mechanical properties
1654 of plasma membrane vesicles correlate with lipid order, viscosity and cell density.
1655 *Communications Biology*, *2*(1), 1–8. https://doi.org/10.1038/s42003-019-0583-3
1656 Strulson, M. K., & Maurer, J. A. (2011). Microcontact printing for creation of patterned lipid
1657 bilayers on tetraethylene glycol self-assembled monolayers. *Langmuir : The ACS*
1658 *Journal of Surfaces and Colloids*, *27*(19), 12052–12057.
1659 https://doi.org/10.1021/la201839w
1660 Sullan, R M A, Li, J. K., Hao, C. C., Walker, G. C., & Zou, S. (2010). Cholesterol-Dependent
1661 Nanomechanical Stability of Phase-Segregated Multicomponent Lipid Bilayers.
1662 *Biophysical Journal*, *99*(2), 507–516. https://doi.org/10.1016/j.bpj.2010.04.044
1663 Sullan, Ruby May A, Li, J. K., & Zou, S. (2009a). Direct Correlation of Structures and
1664 Nanomechanical Properties of Multicomponent Lipid Bilayers. *Langmuir*, *25*(13), 7471–
1665 7477. https://doi.org/10.1021/la900395w
1666 Sullan, Ruby May A, Li, J. K., & Zou, S. (2009b). Quantification of the Nanomechanical Stability
1667 of Ceramide-Enriched Domains. *Langmuir*, *25*(22), 12874–12877.
1668 https://doi.org/10.1021/la903442s
1669 Sun, M., Graham, J. S., Hegedüs, B., Marga, F., Zhang, Y., Forgacs, G., & Grandbois, M. (2005).
1670 Multiple Membrane Tethers Probed by Atomic Force Microscopy. *Biophysical Journal*,
1671 *89*(6), 4320–4329.
1672 Tabaei, S. R., Gillissen, J. J. J., Vafaei, S., Groves, J. T., & Cho, N.-J. (2016). Size-dependent,
1673 stochastic nature of lipid exchange between nano-vesicles and model membranes.
1674 *Nanoscale*, *8*(27), 13513–13520. https://doi.org/10.1039/C6NR03817D
1675 Tellechea, E., Johannsmann, D., Steinmetz, N. F., Richter, R. P., & Reviakine, I. (2009). Model-
1676 Independent Analysis of QCM Data on Colloidal Particle Adsorption. *Langmuir*, *25*(9),
1677 5177–5184. https://doi.org/10.1021/la803912p

1678 Tero, R. (2012). Substrate Effects on the Formation Process, Structure and Physicochemical
1679 Properties of Supported Lipid Bilayers. *Materials*, *5*(12), 2658–2680.
1680 https://doi.org/10.3390/ma5122658
1681 Van Lehn, R. C., Ricci, M., Silva, P. H. J., Andreozzi, P., Reguera, J., Voïtchovsky, K., Stellacci, F.,
1682 & Alexander-Katz, A. (2014). Lipid tail protrusions mediate the insertion of
1683 nanoparticles into model cell membranes. *Nature Communications*, *5*(1), 4482.
1684 https://doi.org/10.1038/ncomms5482
1685 van Meer, G., & de Kroon, A. I. P. M. (2011). Lipid map of the mammalian cell. *Journal of Cell*
1686 *Science*, *124*(1), 5.
1687 van Meer, G., Voelker, D. R., & Feigenson, G. W. (2008). Membrane lipids: Where they are and
1688 how they behave. *Nature Reviews Molecular Cell Biology*, *9*(2), 112–124.
1689 https://doi.org/10.1038/nrm2330
1690 Veatch, S. L., & Keller, S. L. (2003). Separation of Liquid Phases in Giant Vesicles of Ternary
1691 Mixtures of Phospholipids and Cholesterol. *Biophysical Journal*, *85*(5), 3074–3083.
1692 Vereb, G., Szöllősi, J., Matkó, J., Nagy, P., Farkas, T., Vígh, L., Mátyus, L., Waldmann, T. A., &
1693 Damjanovich, S. (2003). Dynamic, yet structured: The cell membrane three decades
1694 after the Singer–Nicolson model. *Proceedings of the National Academy of Sciences*,
1695 *100*(14), 8053 LP – 8058. https://doi.org/10.1073/pnas.1332550100
1696 Vist, M. R., & Davis, J. H. (1990). Phase equilibria of cholesterol/dipalmitoylphosphatidylcholine
1697 mixtures: Deuterium nuclear magnetic resonance and differential scanning
1698 calorimetry. *Biochemistry*, *29*(2), 451–464. https://doi.org/10.1021/bi00454a021
1699 Vogel, V. (2006). MECHANOTRANSDUCTION INVOLVING MULTIMODULAR PROTEINS:
1700 Converting Force into Biochemical Signals. *Annual Review of Biophysics and*
1701 *Biomolecular Structure*, *35*(1), 459–488.
1702 https://doi.org/10.1146/annurev.biophys.35.040405.102013

Voinova, M. V., Rodahl, M., Jonson, M., & Kasemo, B. (1999). Viscoelastic Acoustic Response of Layered Polymer Films at Fluid-Solid Interfaces: Continuum Mechanics Approach. *Physica Scripta*, *59*(5), 391. https://doi.org/10.1238/Physica.Regular.059a00391

Wallace, E. J., Hooper, N. M., & Olmsted, P. D. (2006). Effect of hydrophobic mismatch on phase behavior of lipid membranes. *Biophysical Journal*, *90*(11), 4104–4118. https://doi.org/10.1529/biophysj.105.062778

Wargenau, A., & Tufenkji, N. (2014). Direct Detection of the Gel–Fluid Phase Transition of a Single Supported Phospholipid Bilayer Using Quartz Crystal Microbalance with Dissipation Monitoring. *Analytical Chemistry*, *86*(16), 8017–8020. https://doi.org/10.1021/ac5019183

Winkler, P. M., Campelo, F., Giannotti, M. I., & García-Parajo, M. F. (2020). Planar plasmonic antenna arrays resolve transient nanoscopic heterogeneities in biological membranes. *Proc.SPIE*, *11246*. https://doi.org/10.1117/12.2543726

Winkler, P. M., Regmi, R., Flauraud, V., Brugger, J., Rigneault, H., Wenger, J., & García-Parajo, M. F. (2017). Transient Nanoscopic Phase Separation in Biological Lipid Membranes Resolved by Planar Plasmonic Antennas. *ACS Nano*, *11*(7), 7241–7250. https://doi.org/10.1021/acsnano.7b03177

Yeagle, P. L. (1989). Lipid regulation of cell membrane structure and function. *The FASEB Journal*, *3*(7), 1833–1842. https://doi.org/10.1096/fasebj.3.7.2469614

Zou, S., & Johnston, L. J. (2010). Ceramide-enriched microdomains in planar membranes. *Current Opinion in Colloid & Interface Science*, *15*(6), 489–498. https://doi.org/10.1016/j.cocis.2010.06.003

1729